Understanding caldera structure and development: An overview of analogue models compared to natural calderas

Valerio Acocella *

Dipartimento Scienze Geologiche Roma Tre, Roma, Italy

Abstract

Understanding the structure and development of calderas is crucial for predicting their behaviour during periods of unrest and to plan geothermal and ore exploitation. Geological data, including that from analysis of deeply eroded examples, allow the overall surface setting of calderas to be defined, whereas deep drillings and geophysical investigations provide insights on their subsurface structure. Collation of this information from calderas worldwide has resulted in the recent literature in five main caldera types (downsag, piston, funnel, piecemeal, trapdoor), being viewed as end-members. Despite its importance, such a classification does not adequately examine: (a) the structure of calderas (particularly the nature of the caldera's bounding faults); and (b) how this is achieved (including the genetic relationships among the five caldera types). Various sets of analogue models, specifically devoted to study caldera architecture and development, have been recently performed, under different conditions (apparatus, materials, scaling parameters, stress conditions).

The first part of this study reviews these experiments, which induce collapse as a result of underpressure or overpressure within the chamber analogue. The experiments simulating overpressure display consistent results, but the experimental depressions require an exceptional amount of doming, seldom observed in nature, to form; therefore, these experiments are not appropriate to understand the structure and formation of most natural calderas. The experiments simulating underpressure reveal a consistent scenario for caldera structure and development, regardless of their different boundary conditions. These show that complete collapse proceeds through four main stages, proportional to the amount of subsidence, progressively characterized by: (1) downsag; (2) reverse ring fault; (3) peripheral downsag; (4) peripheral normal ring fault.

The second part of this study verifies the possibility that these latter calderas constitute a suitable analogue to nature and consists of a comprehensive comparison of the underpressure experiments to natural calderas. This shows that all the experimental structures, as well as their progressive development, are commonly observed at natural calderas, highlighting a consistency between models and nature. As the shallow structure of experimental calderas corresponds to a precise architecture at depth, it provides a unique key to infer the deeper structure of natural calderas: recognizing diagnostic surface features within a caldera will thus allow it to be categorized within a precise structural and evolutionary context. The general relationship between the evolutionary stage of a caldera and its d/s (diameter/subsidence) ratio allows such a quantification, with stage 1 calderas characterized by d/s>40, stage 2 by 18<d/s<40, stage 3 by 14<d/s<18 and stage 4 by d/s<14. The consistency between experiments and nature suggests that, in principle, the d/s ratio may permit to evaluate the overall structure and evolutionary stage of a caldera even when its surface structure is poorly known. The volume of erupted magma associated with caldera collapse is poorly dependent on the d/s ratio or evolutionary stage; however, the location of sin- and post-collapse volcanism may depend not only upon the amount of collapse, but also on the roof aspect ratio. As the regional tectonic control is concerned, the experiments

---

* Fax: +39 6 54888201.
 E-mail address: acocella@uniroma3.it.

explain the ellipticity of a part of natural calderas elongated parallel to the regional extension; the control of pre-existing structures may explain the elongation of elliptic calderas oblique or parallel to the regional structures.

The four stages adequately explain the architecture and development of the established caldera end-members along a continuum, where one or more end-members (downsag, piston, funnel, piecemeal, trapdoor) may correspond to a specific stage. While such a continuum is controlled by progressive subsidence, specific collapse geometries will result from secondary contributory factors (roof aspect ratio, collapse symmetry, pre-existing faults). These considerations allow proposing an original classification of calderas, incorporating their structural and genetic features.

1. Introduction

Collapse calderas are subcircular depressions, in volcanic areas, whose diameter is considered to be larger than that of explosive vents and craters (Williams, 1941), possibly reaching many tens of km, as La Garita (USA, Lipman, 2003). Calderas may be characterized by a variable amount of subsidence, ranging from few m to few km. Their shape may be subcircular, or more commonly elliptical, possibly reflecting the influence of a regional tectonic control (Holohan et al., 2005, and references therein). Calderas are formed under various tectono-magmatic conditions, as along felsic (or silicic) volcanic arcs in convergent settings (De Silva, 1989; Cole, 1990; Yoshida, 2001), mafic and felsic oceanic and continental divergent settings (Mohr and Wood, 1976; Gudmundsson, 1998a; Bosworth et al., 2003), felsic strike-slip settings (Bellier and Sebrier, 1994) and mafic hot spots (Newhall and Dzurisin, 1988, and references therein). Despite this variability, there is a tendency for felsic explosive eruptions to be related to calderas formed in a shorter time span (hours to days), triggering catastrophic events. Conversely, moderate effusive mafic activity is usually associated with calderas formed over broader time spans (days to years; Newhall and Dzurisin, 1988, and references therein).

Two mechanisms have been proposed to explain caldera formation. In the most popular model, calderas are the surface expression of the emptying of the magma chamber during effusive or explosive eruptions. As a result of an underpressure within the magma chamber at some point before the collapse, the roof of the reservoir yields, forming a depression at surface (Williams, 1941; Druitt and Sparks, 1984; Branney, 1995; Lipman, 1997). The mass fraction of magma that must be erupted to induce collapse varies between a few percent to 40%; once initiated, collapse will tend to force out most or all of the volatile-rich magma from the chamber (Martì et al., 2000). The alternative mechanism explains caldera collapse as a result of an overpressure within the chamber; the overpressure induces doming and subsequent apical tensile stresses, which may lead to the initiation of collapse (Gudmundsson, 1988; Gudmundsson et al., 1997; Burov and Guillou-Frottier, 1999; Guillou Frottier et al., 2000).

The common association between caldera formation and eruptions is one of the main motivations to study their structure and development; in fact, predicting the possible structural control on the behaviour of calderas during periods of unrest may help in mitigating the hazard. In addition, understanding the structure of calderas is important to plan geothermal and ore exploitation (Stix et al., 2003).

The variety of caldera size, subsidence, shape, tectonic environment and composition of the related magmas, as well as the debated mechanism of formation, are the main factors that for decades have hindered the formulation of a comprehensive model to describe caldera structure and development. Other factors are the lack of direct observations of caldera formation and the difficulty of defining the deeper structure, even at the best-exposed active calderas on Earth, such as Kilauea, Hawaii or Erta Ale, Ethiopia (Fig. 1).

A first approach to systematic understanding of caldera subsidence has been to define, largely based on field, drilling and geophysical data, discrete end-member types with distinct geometric, evolutionary and eruptive characteristics (Walker, 1984; Lipman, 1997; Kennedy and Styx, 2003; Cole et al., 2005). Primarily based on field data, five end-member caldera geometries or styles (piston, piecemeal, trapdoor, downsag, funnel) have been proposed (Fig. 2; e.g. Lipman, 1997) and commonly referred to in the literature (e.g. Cole et al., 2005, and references therein). Piston-type calderas are bordered by a ring fault, delimiting the sinking central block; piecemeal collapses result from the differential vertical movement of multiple independent blocks; trapdoor collapses are asymmetric depressions, with an unfaulted hinge; downsag calderas are broad depressions characterized by inward tilted margins; funnel calderas are narrow and

deep cone-shaped depressions, often associated with gravitational slumping (Fig. 2).

However, such an end-member classification may be too restrictive and not as useful in documenting a collapse style, which may correspond to different morphologies at the surface (Cole et al., 2005). In addition, there are many unanswered questions, including: (a) means of accommodation of subsidence at depth, which concerns the resolution of the "room problem" (how the subsidence of the central block is accommodated at crustal depths); (b) nature (geometry and kinematics) of the caldera's bounding faults; (c) mechanism of development of the five established caldera types and their possible relationships (as little is known on the conditions leading to a certain type of caldera and its genetic relationships with the other types). All these issues can only be adequately explained if both the structure and mechanism of development of calderas, which are closely related, are understood.

This study constrains the structure and development of calderas through an overview of analogue experiments and a comprehensive comparison with examples of calderas. Several sets of analogue experiments have been performed in the last few years, to simulate collapse calderas. These have been run under different conditions, providing a valuable data set. Most of these studies have focused mainly on the experimental results themselves, rather than on the comparison to actual examples; as a result, these experiments are probably still being considered below their potential by the volcanological community. The aim of this study is to: (a) give a comprehensive overview of all the experiments, highlighting similarities and differences regarding the structure of calderas and their mechanism of formation; (b) propose a structural evolutionary model, consistent with all the experimental data sets; (c) reconcile this model with the available geological, geophysical and numerical data, to provide tools to understand the structure and mechanism of formation of a significant part of the known calderas; (d) propose, by comparison between models and actual examples, an updated genetic caldera classification.

Calderas are here considered to be those depressions resulting from an underpressure and/or overpressure within the magma chamber. This includes both mafic and felsic calderas, regardless of their tectonic setting, ellipticity and amount of subsidence. Moreover, as pit craters (collapses, with a diameter from a few m to several hundreds of m, deriving from the emplacement of lava below; Okubo and Martel, 1998, and references therein) are inferred to share a common origin to calderas, this study includes pit craters, covering the full spectrum of magma-induced collapses in volcanic areas. As the struc-

ture of calderas may be controlled by regional tectonics (e.g. Bosworth et al., 2003), this work also considers the effect of regional stresses and pre-existing structures. The terminology used here refers to that previously defined in Lipman (1997) and Cole et al. (2005).

2. Available data on caldera structure

This section summarizes the main results from geological (including studies from eroded calderas; Section 2.1), geophysical (Section 2.2) and numerical (Section 2.3) studies devoted at defining the structure of calderas and pit craters.

2.1. Geological data

The calderas at divergent settings, as along the rift zones of Kenya, Ethiopia and Iceland, usually show a sharp rim (morphological expression of the structural margin), with piston-like structures, often complicated by nested collapses (Williams et al., 1984; Acocella et al., 2002, and references therein; Bosworth et al., 2003, and references therein; Gudmundsson and Nilsen, 2006). Similarly, at hot spots (as Hawaii, Galapagos and Canarias), calderas usually resemble piston-like structures, with moderate dimensions and subsidence (Simkin and Howard, 1970; Newhall and Dzurisin, 1988; Chadwick and Howard, 1991; Rowland and Munro, 1992). Polyphased collapses may develop elongated structures, as at Las Canadas (Tenerife, Canarias; Martì and Gudmundsson, 2000). Calderas at convergent settings, as along the Tyrrhenian margin of central Italy (Acocella and Funiciello, 2006, and references therein), NE Honshu (Japan; Yoshida, 2001, and references therein), Taupo Volcanic Zone (New Zealand; Spinks et al., 2005, and references therein) and the Central Andes (De Silva, 1989, and references therein) show less defined rims, possibly due to the later explosive activity. Common features are the large dimensions (diameters usually >10 km), with a significant subsidence (up to a few km), also depending on their location within the rift zone axis (Spinks et al., 2005). Post-caldera resurgence is common, as at Campi Flegrei and Ischia (Italy; Vezzoli, 1988; Orsi et al., 1996), Amatitlan (Guatemala; Wunderman and Rose, 1984) and La Pacana (Chile; Lindsay et al., 2001).

Active calderas, such as Long Valley, Valles, Kilauea and Mauna Loa (USA), Krafla (Iceland) and Campi Flegrei (Italy) are among the best studied. Despite the debated nature of the Campi Flegrei area (De Vivo et al., 2001; Rolandi et al., 2003; Bellucci et al., 2006), surface and subsurface data confirm the presence of a nested collapse structure, ~2 km deep (Acocella and Faccenna,
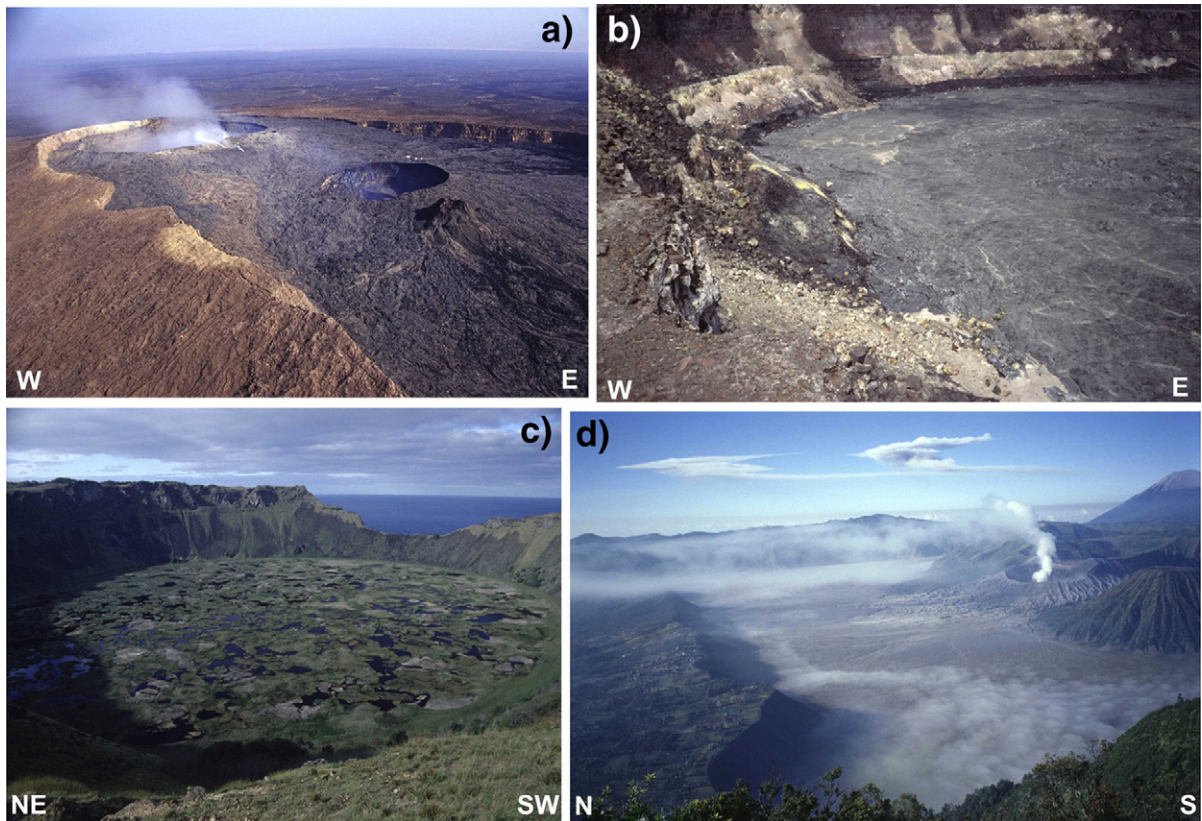
Fig. 1. Surface structure of some of the best exposed active calderas on Earth: (a) Erta Ale, Afar, Ethiopia; (b) detail of the SW rim of Kilauea; (c) Rano Kau caldera; Easter Island, Chile; (d) N rim of Bromo caldera, Indonesia. Here the surface structure (rim configuration, eccentricity, amount of subsidence) of a caldera may be evaluated, but it is still not possible to define the deeper structure and how and why this developed.

2007), consistently with previous studies (Rosi and Sbrana, 1987; Barberi et al., 1991; Orsi et al., 1996; Florio et al., 1999). Valles also has a ∼2 km deep and articulated caldera floor, with nested structures (Self et al., 1986; Self and Wolff, 2005, and references therein), whereas Long Valley resembles an asymmetric piston-like structure (Bailey et al., 1976; Goldstein and Stein, 1988, and references therein; Suemnicht and Varga, 1988). The active calderas with mainly basaltic effusive activity (Mauna Loa, Kilauea, Krafla) have a simpler piston-like structure, with lower subsidence (very few hundreds of meters), locally complicated by pit craters (Newhall and Dzurisin, 1988, and references therein; Gudmundsson and Nilsen, 2006). One place where shallow internal structures can be seen is at Miyakejima, Japan, where two nested depressions, bordered by reverse (formed first) and normal faults, formed in 2000 (Fig. 3a and b; Geshi et al., 2002).

As an example of a pit crater, the Santiago pit is bordered by outward dipping reverse faults, culminating in an inward tilt at the surface (Rymer et al., 1998; Roche et al., 2001). Subvertical to outward dipping walls are also observed at the Erta Ale pit, Afar, hosting the lava lake (Acocella, 2006a) and inferred at the Dolomieu pit at Piton de la Fournaise (Reunion Island; Carter et al., 2007). Ice-melt collapse pits and mining-subsidence structures, 1–15 m wide, are also bordered by outward dipping reverse faults (Branney, 1995; Branney and Gilbert, 1995).

Many partially eroded calderas allow direct information on the deeper structure, as at Gran Canaria (Canary Islands, Schmincke, 1967), Western United States (Lipman, 1984; Rytuba and McKee, 1984), Trans Pecos (Texas; Henry and Price, 1984), Sierra Madre Occidental (Mexico; Swanson and McDowell, 1984), Tavua (Fiji; Setterfield et al., 1991), Scafell (England; Branney and Kokelaar, 1994), Dorobu and Kumano (Japan; Miura and Tamai, 1998; Miura, 1999; Miura, 2005), Glencoe and Rum (Scotland; Moore and Kokelaar, 1998; Troll et al., 2000), Hannegan (Tucker et al., 2007) and the Archean Hunter Mine Group (Canada; Mueller and Mortensen, 2002). Among these, Kumano and Hannegan reveal trapdoor collapses (Miura, 2005; Tucker et al., 2007), and Scafell and Glencoe a piecemeal-like structure, consisting
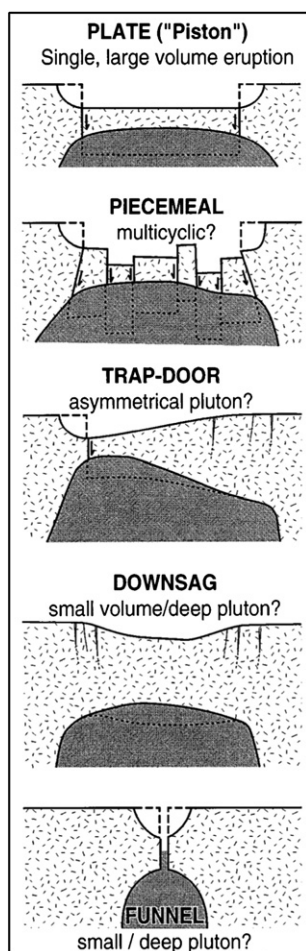
Fig. 2. Established caldera end-members proposed in the literature (after Lipman, 1997; Cole et al., 2005).

of a broad downsag, locally complicated by pre-existing faults accommodating differential displacement (Fig. 3c; Branney and Kokelaar, 1994; Moore and Kokelaar, 1998). The Archean Hunter Mine Group consisted of a caldera bordered by inward dipping normal faults and outward dipping reverse faults (Fig. 3d; Mueller and Mortensen, 2002; Mueller et al., in press).

In synthesis, the geologic data collected on active and eroded calderas so far has only revealed end-member varieties (nested structures, piecemeals, trapdoors and downsag structures) superimposing over the classic piston-like scheme, consistent with recent reviews (Lipman, 1997; Cole et al., 2005). These types suggest an apparent complexity and the lack of a single, simple collapse model. Moreover, there is still fragmented or poor information on the location, geometry and kinematics of the main caldera structures and how these develop.

2.2. Geophysical data

Gravity data have been used to investigate the deeper parts of calderas, as at Long Valley (California; Carle, 1988), Valles (New Mexico; Self and Wolff, 2005, and references therein) Yellowstone (Wyoming; Smith and Braile, 1994, and references therein), Bolsena (Italy; Nappi et al., 1991), Coromandel Peninsula, Taupo, Reporoa, Rotorua and Okataina (New Zealand; Spinks et al., 2005, and references therein; Smith et al., 2006), Sao Miguel (Azores; Montesinos et al., 1999), Hohi Volcanic Zone (Japan; Kusumoto et al., 1999) and Las Canadas (Canary Islands; Camacho et al., 1991; Arana et al., 2000). In some cases, as Campi Flegrei (Italy; Barberi et al., 1991) or Guayabo (Costa Rica; Hallinan, 1993; Hallinan and Brown, 1995), gravity data suggest nested collapses.

Seismicity has been repeatedly used to define caldera structure. At Rabaul, Papua New Guinea, seismicity studies suggest that the caldera is bordered by high angle outward dipping ring faults (Fig. 4a; Mori and Mckee, 1987) or by subvertical to outward dipping structures, associated with compression, in the innermost caldera, and extension, in the outermost caldera (Saunders, 2001). The distribution of seismicity at Pinatubo (Philippines; 1991 eruption) and Mt St Helens (USA; 1980 eruption) suggests the collapse of the chamber roof along outward dipping faults, even though this did not result in the formation of any caldera at the surface (Fig. 4b, c; Scandone and Malone 1985; Mori et al., 1996). Focal mechanisms at Onikobe caldera (Japan) suggest that this is partly bordered by strike-slip faults, consistent with its overall compressional setting (Nakajima and Hasegawa, 2003).

Seismic data at Latera (Italy; Nappi et al., 1991) and Taupo (New Zealand; Davy and Caldwell, 1998) reveal two nested calderas. Okataina (New Zealand; Davy and Bibby, 2005) and Denham (Tonga-Kermadec arc; Worthington et al., 1999, and references therein) show a down-sag structure of portion of the caldera infill.

Tomographic studies permit to define the overall subsurface structure of calderas, as at Campi Flegrei and Vesuvio (Italy; Zollo et al., 1996; Zollo et al., 2003), Rabaul (Papua New Guinea; Bai and Greenlangh, 2005) and Aso (Japan; Sudo and Kong, 2001). However, the resolution (usually > 1 km) is still too low to appreciate the detail of any caldera structure.

In synthesis, most of the geophysical studies permit only a general definition, at the caldera scale, of the configuration of the buried masses. The scale limitation largely results from the inadequate resolution (usually ~ 1 km in gravity and tomography) in detecting caldera structures. More detailed information is limited (Rabaul, Guayabo).
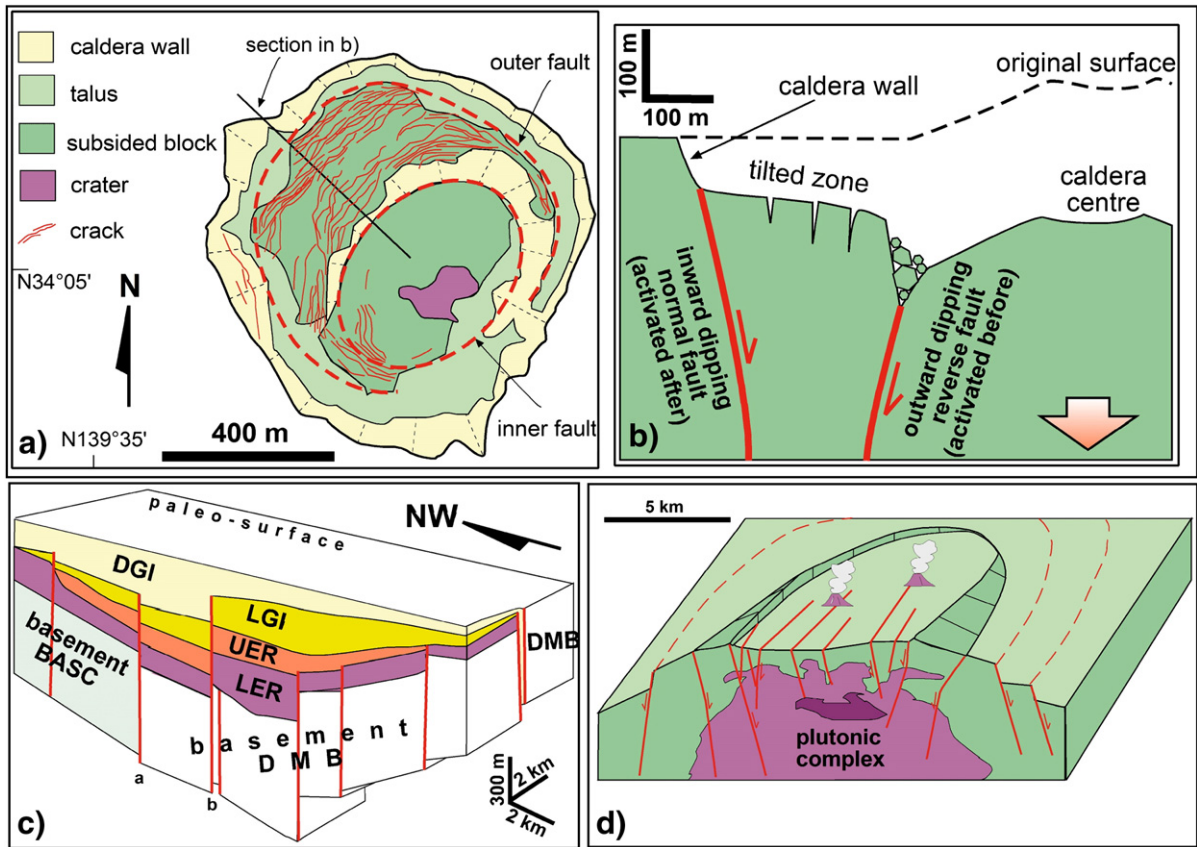
Fig. 3. Examples of geological data on calderas. Map (a) and section (b) view of Miyakejima caldera, Japan, formed in 2000, bordered by reverse faults (formed first) and normal faults (formed later) (modified after Geshi et al., 2002). (c) Schematic structure of Glencoe caldera, England, and its main units, with a piecemeal-like structure (modified after Moore and Kokelaar, 1998). (d) Schematic reconstruction of the Archean Hunter Mine Group caldera, Canada, with inward dipping normal faults and outward dipping reverse faults (modified after Mueller and Mortensen, 2002).

2.3. Numerical models

Numerical models concerning the structure and development of calderas are considered for a comparison with the analogue results and actual examples.

Boundary element models have been used to understand caldera fault initiation considering pressure variations of a cavity in an elastic plate (Fig. 5a; Gudmundsson et al., 1997; Gudmundsson, 1998b). These suggest that a sill-like magma chamber subject to doming, when the doming area is much larger than that of the reservoir, induces a stress field suitable for the initiation at surface of a normal ring fault bordering the caldera. Models with an elastic–plastic–ductile rheology show that, without a regional stress field, collapse along upward-propagating subvertical to inward dipping caldera faults may occur, at the sides of the chamber, only for aspect ratios (thickness/ width) of the chamber roof <0.2; conversely, a regional stress field induces the localization of the faults in the central part of the chamber roof (Burov and Guillou-Frottier, 1999). Kusumoto and Takemura (2003) simulated the collapse through the contraction of a small sphere in an elastic medium, forming an outward dipping reverse ring fault and a peripheral inward dipping normal ring fault. Elastic models simulating pressure variations within a reservoir suggest that normal faults bordering a caldera may form under regional extension (Gray and Monaghan, 2004). Thermoelastic models show a distinct geometry of the caldera ring faults, depending on the aspect ratio of the chamber roof and the eccentricity of the chamber: normal faults form with lower aspect ratios of the roof chamber and sill-like calderas, whereas it is inferred that reverse faults may form with higher roof aspect ratios (Folch and Martì, 2004). Elastic models simulating pressure variations within a reservoir suggest that normal faulting during caldera collapse initiates at surface and depends on the presence and shape of volcanic edifices (Pinel and Jaupart, 2005).
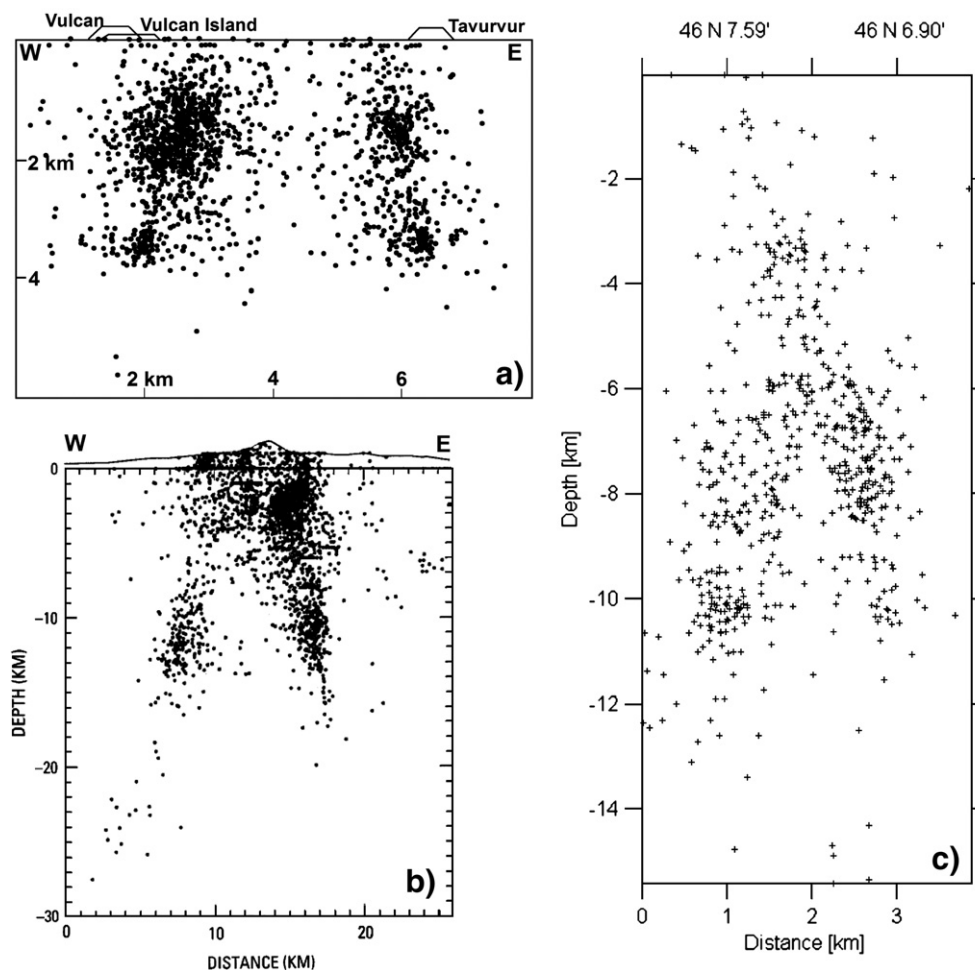
Fig. 4. a) Example of geophysical data on volcanoes. (a) Outward dipping faults highlighted by the distribution of seismicity at Rabaul (section view; modified after Mori and Mckee, 1987). (b) and (c) Depth distribution of syn- and post-eruption earthquakes at Pinatubo (in 1991; b) and Mt St Helens (in 1980; c); the seismic-free zone is interpreted to correspond to the magma chamber (after Scandone and Malone 1985; Mori et al., 1996). The distribution of the seismicity suggests the collapse of the chamber roof along outward dipping faults during the eruption, even though this did not result in the formation of any caldera at the surface.

In synthesis, the numerical models give controversial information, depending on the imposed conditions and assumptions, on the structure and development of calderas. Several elastic models, pressurizing a reservoir analogue (Gudmundsson et al., 1997; Gudmundsson, 1998b; Folch and Martì, 2004; Gray and Monaghan, 2004; Pinel and Jaupart, 2005), suggest that caldera collapse produces downward propagating normal faults. Elastic–plastic–ductile models (Burov and Guillou-Frottier, 1999) suggest that the normal and subvertical faults are upward propagating. Other elastic models, simulating volume variations in the reservoir (Kusumoto and Takemura, 2003), suggest that upward propagating reverse and normal faults develop.

2.4. Analogue models

This overview shows that the structure of some calderas is sufficiently known to reveal variations (nested structures, piecemeals, trapdoors, downsags) from the simple piston-like model. This stimulates better definition of a structural model and the genetic relationships between caldera types. At a more detailed scale, our knowledge on the formation, location, geometry and kinematics of the subsurface structure of calderas is still inadequate, both in terms of resolution and fragmentation of the data. These facts highlight the importance of modelling exclusively aimed at structure. A critical overview, re-evaluation and comparison of the several
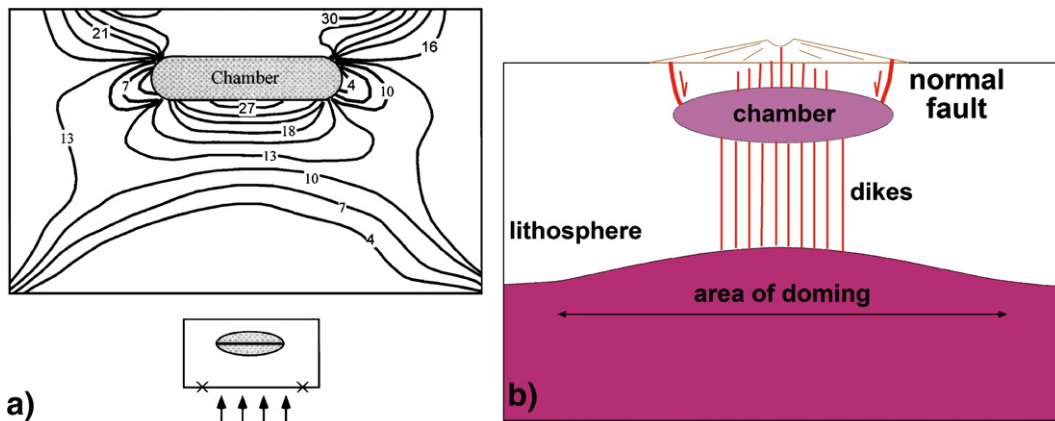
Fig. 5. (a) Example of numerical models on calderas. The maximum stress around a sill-like magma chamber subject to basal doming encourages the initiation of normal faults (values in MPa); (b) possible corresponding situation (modified after Gudmundsson et al., 1997; Gudmundsson, 1998b).

sets of analogue models recently reported is therefore important to advance our knowledge on the structure and development of calderas.

3. Analogue modelling, materials and scaling

Analogue modelling is a scaled simulation of the natural processes. The models simulate the mechanism of collapse, defining the evolution of the deformation and the role of the different parameters controlling the deformation, applicable to a wide range of examples. The main advantage is the direct observation of the deformation in 3D, at an accessible scale (mm to m), within a reasonable time span (minutes to days). Moreover, analogue models provide discontinuous solutions, such as the development of faults, and are particularly suitable to reconstruct mechanisms of deformation and associated structural patterns. The greatest limitation is the current difficulty of simulating temperature gradients. As a result, analogue caldera modelling simulates a system with 2 components, a magma chamber below a brittle upper crust. The volume variation of the reservoir analogue induces deformation in the brittle material, while any ductile crust overlying the magma chamber is neglected. This limitation is not considered crucial, as several geophysical studies suggest that the behaviour of the crust may be often approximated brittle (Cespuglio et al., 1996; Natale et al., 2005; Guidarelli et al., 2006; Nunziata et al., 2006). Another common assumption is that the simulated contraction of the magma chamber is related to the extrusion of magma. However, the development of a conduit feeding a vent and extruding magma, as well as its interaction with the collapse, cannot be currently reproduced experimentally. As the experiments are simply focused on the effect of

magma withdrawal, that is the contraction of the magma chamber analogue, these limitations are not considered crucial to study caldera collapse.

The modelling aims at the geometric, kinematic and dynamic similarity with nature (Hubbert, 1937; Ramberg, 1981), which is obtained through precise scaling proportions, in the choice of both the analogue materials and the apparatus. The brittle crust is usually simulated by sand, flour or clay. Their choice depends upon the imposed length ratio between model and nature, L^*, which affects the cohesion of the crustal analogue. In most experiments, for practical reasons, $L^* \sim 10^{-5}$; moreover, the density ratio between rocks and experimental materials is $\rho^* \sim 0.5$ and the gravity ratio between model and nature is $g^* = 1$. Therefore, the stress ratio between model and nature is $\sigma^* = \rho^* g^* z^* \sim 5 \times 10^{-6}$ (Table 1). As the cohesion c^* has the dimensions of stress, assuming a Mohr–Coulomb criterion and a cohesion $c \sim 10^7$ Pa for the rocks, a material with $c \sim 50$ Pa is required to simulate the brittle crust. The most suitable material is dry quartz sand, with a negligible cohesion (a few Pa), a Mohr–Coulomb failure criterion similar to the rocks in the brittle crust and an angle of internal friction $\phi \sim 30°$. Flour and clay have slightly larger cohesion (1–3 orders of magnitude) and are not ideal crust analogues. Nevertheless, if added in small quantities ($\leq 10\%$) to sand, they may increase its elastic behaviour and enhance the resolution and details of the structures (as subvertical scarps and extension fractures; Donnadieu and Merle, 1998).

The magma chamber responsible for collapse has been simulated by air, water and silicone. The main difference in these materials lies in their viscosity (μ), ranging from 10^{-5} (air) to 10^{-3} (water) and 10^4 (silicone) Pa s. The viscosity of magma can vary over 12 orders of magnitude, depending on its composition and temperature (Talbot,

1999). Ideally, using a certain magma analogue, it is possible to simulate a wide range of viscosities, by controlling strain rate ratios ε^* ($\varepsilon^* = \sigma^*/\mu^*$), time ratios t^* ($t^* = 1/\varepsilon^*$) and velocity of deformation ratios v^* (Table 1; Merle and Vendeville, 1995). In practice, all the used magma analogues have some advantage and limitation. While silicone may be ideal to simulate viscous magmas ($\mu \sim 10^{10}$ Pa s), the lower viscosity of air and, mostly, water is more suitable to simulate basaltic magmas. However, unlike silicone, their confinement within a balloon limits their flow, mobility and attitude to intrude.

4. Experimental studies on calderas

4.1. General features

This section considers the analogue studies simulating calderas, due to overpressure or underpressure conditions within the reservoir, following the two triggering mechanisms proposed in Section 1. The whole experimental set, consisting of 16 studies (Table 2), is therefore grouped into two categories. (a) Experiments where a form of collapse or depression is achieved through overpressure within the simulated reservoir, even though aimed at investigating pre-collapse tumescence (Komuro et al., 1984; Martì et al., 1994; Walter and Troll, 2001; Troll et al., 2002), resurgence or pluton emplacement (Acocella et al.; 2001a; Acocella and Mulugeta, 2002), and not caldera formation. As all these studies, despite their original aim, obtained a depression as a result of the emplacement of a magma analogue, they are included in the overpressure category. (b) Experiments where the collapse is achieved through underpressure within the simulated magma chamber (Komuro, 1987; Martì et al., 1994; Acocella et al., 2000; Roche et al., 2000; Acocella et al., 2001b; Walter and Troll, 2001; Troll et al., 2002; Kennedy et al.,

2004; Lavallèe et al., 2004; Belousov et al., 2005; Geyer et al., 2006). This category includes experiments of collapse under a regional stress field (Cailleau et al., 2003; Acocella et al., 2004; Holohan et al., 2005). Martì et al. (1994), Walter and Troll (2001) and Troll et al. (2002) in (a) also appear in (b), as they simulated both underpressure and overpressure conditions.

4.2. Collapse induced by overpressure

Komuro et al. (1984) have modelled a collapse basin related to magma emplacement with a rigid sphere (magma chamber analogue) rising within a box of dry sand and clay in different proportions (brittle crust analogue) (Fig. 6a). The surface deformation consists of radial and, subsequently, concentric cracks (Fig. 6b). A broad dome forms; its crest undergoes a subsidence, with the collapsed area bordered by the radial and concentric cracks. The depth of the polygonal collapsed area is a fraction of the dome height, whereas its width is approximately half that of the dome (Fig. 6b).

Martì et al. (1994) simulate doming by inflating (pumping air) an elastic balloon (magma chamber analogue) within fused alumina powder (upper crust analogue) (Fig. 7a). Doming is achieved through high angle inward dipping reverse faults (Fig. 7b). The crest of the dome displays a tensile area, with inward dipping normal faults, the width and depth of which are a fraction of that of the dome.

Walter and Troll (2001) and Troll et al. (2002) use an inflated oblate (or sill-like shaped) balloon, containing air or water (magma chamber analogue) within a sand or flour model (upper crust analogue) (Fig. 8a). The cohesion of flour is larger than that of the sand and its strength is larger than that required to simulate the brittle crust. However, flour allows study of the deformation pattern in more detail and the overall pattern obtained with flour and sand is identical. Inflating the reservoir, the dome is limited by inward-dipping reverse faults (Fig. 8b). Its crest undergoes extension and subsidence, developing radial extension fractures and tangential extension fractures. The depth of the crestal depression is a fraction of the height of the dome, whereas its width is several times narrower than the dome.

Acocella et al. (2001a) simulate resurgence (consisting of a localized uplift of a volcanic system; Lipman, 1984 and references therein) due to shallow magma emplacement. Newtonian silicone (magma analogue) rises below a sand-pack (brittle crust analogue), simulating an overpressure within the reservoir. With roof aspect ratios $A < 0.8$ (A = thickness/width) a broad dome, with peripheral inward dipping reverse faults, forms (Fig. 9). After

Table 1
Parameters scaled to simulate the brittle crust and the ductile magma chamber during caldera collapse (modified after Merle and Vendeville, 1995)

Parameter	Model/nature ratio
Brittle crust	
Length	L^*
Density	ρ^*
Gravity	g^*
Stress	$\sigma^* = \rho^* g^* L^*$
Cohesion	$c^* = \sigma^*$
Magma	
Viscosity	μ^*
Strain rate	$\varepsilon^* = \sigma/\mu$
Time	$t^* = 1/\varepsilon^*$
Velocity	$V^* = \varepsilon^* L^*$

Table 2
Performed experiments on calderas, simulating overpressure and underpressure within the chamber analogue and a regional stress field

Category of experiment	Analogue modelling study	Materials + apparatus	Main results
Overpressure	Komuro et al. (1984)	Rigid sphere rising in powder	Radial + concentric fractures with depression on crest of dome
	Martì et al. (1994)	Balloon inflated in powder	Outward dipping reverse faults and crestal normal faults
	Walter and Troll (2001)	Balloon inflation in flour	Subsidence of crest of dome with normal faults
	Acocella et al. (2001a)	Silicone intruding in sand	Doming, crestal thinning and depression
	Troll et al. (2002)	Balloon inflation in flour	Formation of piecemeal collapses
	Acocella and Mulugeta (2002)	Silicone rising below sand (centrifuge)	Doming, crestal depression bordered by inward dipping normal faults
Underpressure	Komuro (1987)	Dry ice evaporating in powder	Outward dipping reverse faults
	Martì et al. (1994)	Balloon in powder	Outward dipping reverse faults + subvertical faults
	Roche et al. (2000)	Silicone sinking in sand	Outward dipping reverse faults + inward dipping normal faults
			Role of root aspect ratio
			Independence from the reservoir shape
	Acocella et al. (2000)	Silicone sinking in sand	Outward dipping reverse faults + inward dipping normal faults
			Room problem
	Acocella et al. (2001b)	Silicone sinking in sand	Constant architecture of nested calderas
	Walter and Troll (2001)	Balloon deflating in flour	Outward dipping reverse faults + inward dipping normal faults
	Troll et al. (2002)	Balloon deflating in flour	Piecemeal calderas through inflation-deflation cycles
	Kennedy et al. (2004)	Balloon deflating in sand	Reverse faults + normal faults controlled by the shape of chamber roof
	Lavallèe et al. (2004)	Baloon deflating in sand (topography–cones)	Topography may locally vary the shape of calderas
	Geyer et al. (2006)	Balloon in sand	Roof aspect ratio and magma chamber withdrawal
Regional stress	Cailleau et al. (2003)	Balloon deflating in flour (regional stress)	Caldera elongated accordingly with the regional stress
	Acocella et al. (2004)	Silicone sinking in sand (regional pre-existing faults)	Caldera elongation may depend on regional fault reactivation
	Holohan et al. (2005)	Balloon deflating in sand (regional stress)	Elongation of calderas parallel to minimum compression

~1 cm of uplift, a crestal depression is observed, indicating apical extension. The depression, a few mm deep, has a width that is a small fraction of that of the dome.

Acocella and Mulugeta (2002) studied the surface deformation induced by shallow pluton emplacement. Silicone (magma analogue) rises in a centrifuge by means of the density contrast with the surrounding medium, below a sand layer (brittle crust analogue) (Fig. 10a). The length ratio between model and nature is $L^* \sim 10^{-6}$. The emplacement of the silicone below the sand induces doming. The crest of the dome undergoes subsidence, becoming bordered by inward dipping normal faults (Fig. 10b and c). The width of the depression, ~2 mm, is a fraction of that of the domed area.

4.3. Collapse induced by underpressure

Of the 13 experimental sets of this category, 5 are performed by the same research group, with same

materials, apparatus and stress conditions. This reduces to 8 the amount of original key papers to be considered: Komuro (1987), Martì et al. (1994), Acocella et al. (2000), Roche et al. (2000), Walter and Troll (2001) and Kennedy et al. (2004), in absence of regional stresses. In addition, Acocella et al. (2004) and Holohan et al. (2005) study caldera collapse under a regional stress field.

4.3.1. Caldera collapse without regional stress field

Komuro (1987) used dry ice (contracting reservoir analogue) evaporating beneath a mixture of sand and clay (upper crust analogue). Because of the cohesive clay, this mixture is one order of magnitude stronger than required. Evaporation of ice results in the overburden collapse, causing ring fractures at the surface (Fig. 11). These are outward dipping in the central part, formed at early stages, and subvertical at the periphery of the collapse, formed at later stages. The outward dip of the ring faults may permit the intrusion of magma during collapse (Fig. 11).
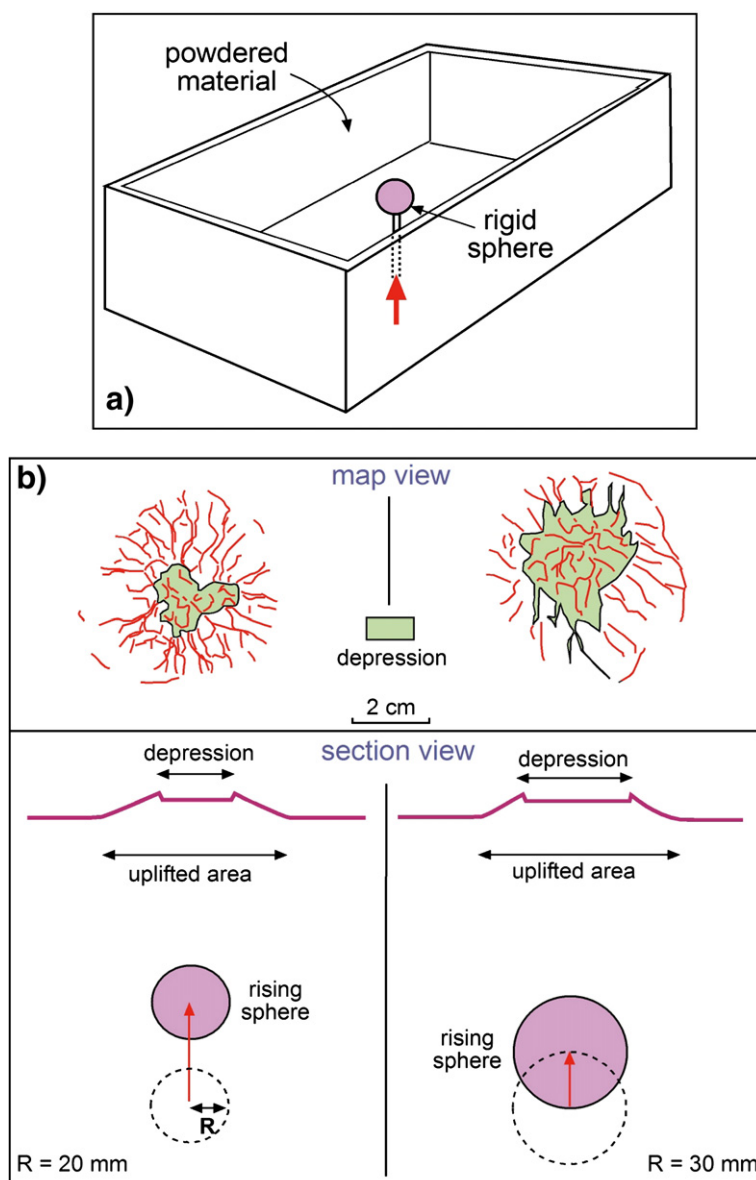
Fig. 6. Overpressure experiments of Komuro et al., 1984. (a) Adopted apparatus; (b) map and section view of two experiments with different chamber radius R (modified after Komuro et al., 1984).

Martì et al. (1994) simulate caldera collapse by deflating (removing air) an elastic balloon (magma chamber analogue) within fused alumina powder (upper crust analogue) (Fig. 7a). Different balloon shapes (spherical, cylindrical, flat, oblate or penny-shaped) simulate different magma chambers. Subsidence develops subvertical faults, which confine an area with several concentric collapsing blocks bordered by outward dipping reverse faults, dying out towards the subvertical faults (Fig. 12). These concentric ring faults suggest that nested calderas may result from a single reservoir.

Roche et al. (2000) is the most detailed and comprehensive experimental study focused on collapses so far. Collapse is achieved by sinking Newtonian silicone (magma analogue) at the base of a sand-pack (brittle crust analogue). The sand-silicone interface is flat or rounded. Sinking is obtained by lowering the height of the top-level of silicone in a tube connected to the main reservoir (Fig. 13a). Several tens of experiments were performed in 2D and 3D, using a wide range of roof aspect ratios (thickness/width 0.2 to 4.5) (Fig. 13b). The general mechanism of collapse is consistent and independent on
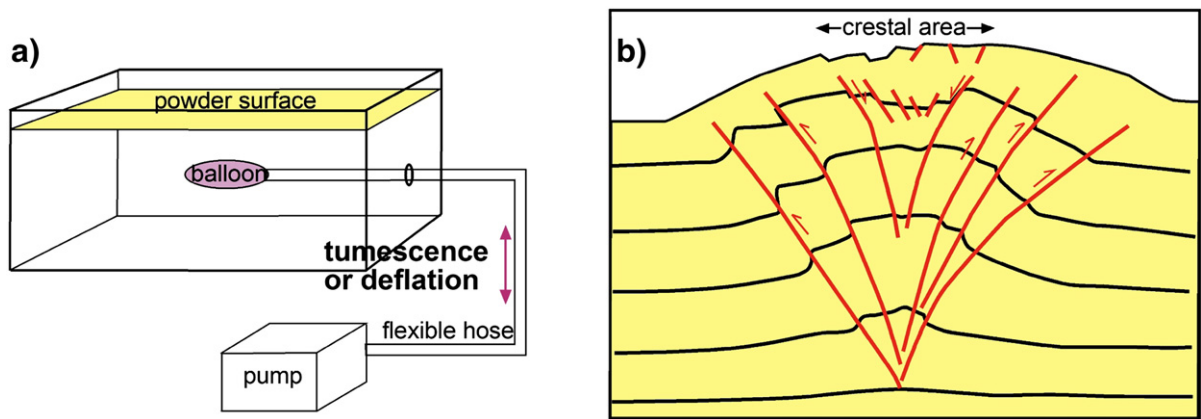
Fig. 7. Overpressure experiments of Martì et al. (1994). (a) Apparatus; (b) section view of a tumescence experiment, characterized by outward dipping reverse faults and a crestal area with subvertical normal faults (modified after Marti et al., 1994).

the map-view shape of the reservoir. For low roof aspect ratios (≤1, type A), subsidence occurs through an inward tilt at surface and the subsequent formation of outward dipping reverse faults (Fig. 13c). When these reach a certain displacement, peripheral inward dipping normal faults form. Inward tilted wedges at surface are bordered
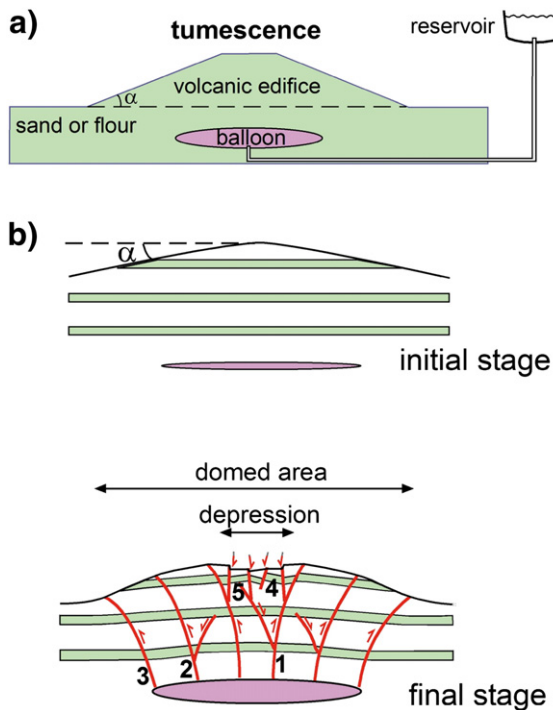

Fig. 8. Overpressure experiments of Walter and Troll (2001). (a) Simplified apparatus, section view; (b) section view of results before and after inflation, with development of an apical depression; numbers 1 to 5 show order of formation of faults (modified after Walter and Troll, 2001).

by the reverse and normal faults, which nucleate at the periphery of the silicone layer. Subsidence usually occurs asymmetrically. These experiments explain the development of coherent piston-like calderas delimited by reverse faults, whereas the gravity-driven normal faults border an outer zone, source of large landslides. For high aspect ratios (≥1, type B), multiple reverse faults propagate upwards concentrically, forming nested cones in an incoherent collapse (Fig. 13c). Normal faults, if present, are restricted to the periphery of the upper cone, where the reverse faults reach surface. These experiments explain the development of funnel-like calderas with minor explosive activity.

Acocella et al. (2000) use Newtonian silicone (same type as Roche et al., 2000) sinking below a sand-pack through a descending piston; various shapes of the sand-silicone interface are considered (Fig. 14a). All the roof aspect ratios fall in the A type of Roche et al. (2000) and the evolution of collapse is also consistent with that of Roche et al. (2000). Two concentric ring faults, the former being reverse and the latter normal, nucleate along the
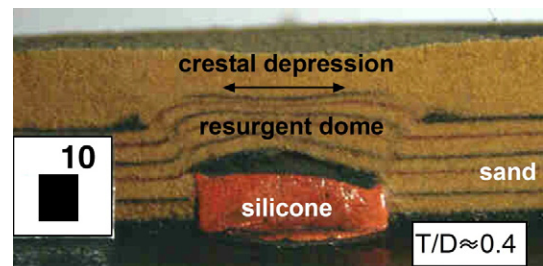

Fig. 9. Overpressure experiments of Acocella et al. (2001a). Lower aspect ratios (T/D, where T=thickness and D=diameter) of the chamber roof develop a crestal depression during resurgence (modified after Acocella et al., 2001a).
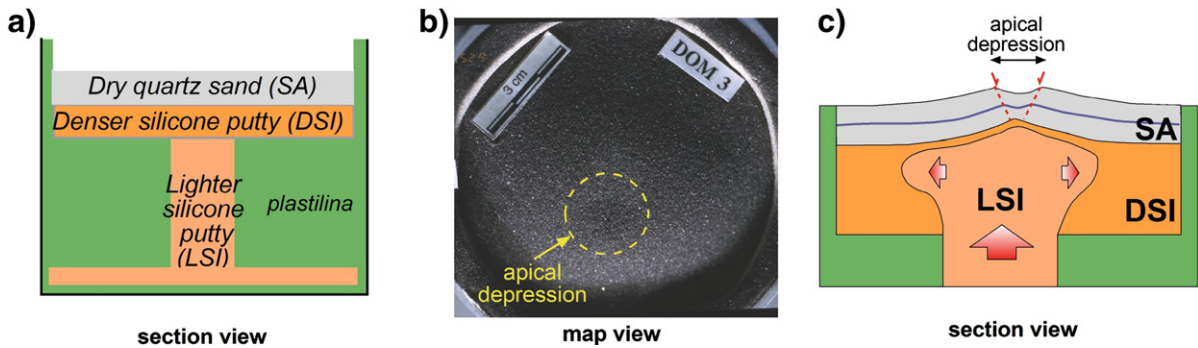
Fig. 10. Overpressure experiments of Acocella and Mulugeta (2002). (a) Apparatus; (b) map and (c) section view of an experiment characterized by doming and apical depression (modified after Acocella and Mulugeta, 2002).

edge of the silicone layer (Fig. 14b). While the reverse faults are due to differential uplift (Sanford, 1959; Mandl, 1988), the normal faults form as a gravitational response. Their combined activity may solve the room problem during large collapses (Fig. 14c). Asymmetric depressions are not common and form only imposing asymmetric silicone domes; these control the location of the maximum point of curvature, that is where the faults nucleate, resulting in faults with different location and amount of slip, generating asymmetric collapses (Fig. 14b; Acocella et al., 2001b). Concentric depressions may explain pairs of natural calderas, as suggested by their constant architecture (Fig. 14d; Acocella et al., 2001b).

Walter and Troll (2001) use a deflating sill-like shaped balloon, containing air or water (magma chamber analogue) within sand or flour (upper crust analogue) (Fig. 15a). The role of a conical volcanic edifice, above the sand pack, is also tested. The evolution of a collapse, consistent with that of Roche et al. (2000) and Acocella et al. (2000), is given by one or more outward dipping reverse faults and peripheral inward dipping normal faults (Fig. 15b). In some cases, the normal faults do not nucleate

directly from the top of the chamber, but in a shallower position. The distribution of the reverse and normal faults is influenced by the morphology of the edifice, when present: steep and irregular flanks result in a tilted and more complex caldera floor. Nevertheless, the overall deformation pattern is consistent with the one observed without volcanic edifices. Inflation and deflation cycles may explain piecemeal collapses, with radial and concentric structures (Troll et al., 2002).

Kennedy et al. (2004) use a ∼ 1 m wide rubber bladder containing water (magma chamber analogue) placed within sand (brittle crust analogue; Fig. 16a). Consistently with what was previously observed (Roche et al., 2000; Acocella et al., 2000; Walter and Troll, 2001), after tilt at surface, concentric outward dipping reverse faults forms (Fig. 16b to f). These nucleate from the centre of the reservoir towards its periphery, following the progressive enlargement of the evacuated area at the top of the dome-shaped bladder (Fig. 16g) and resulting in an outward incremental caldera growth. Subsequently, peripheral
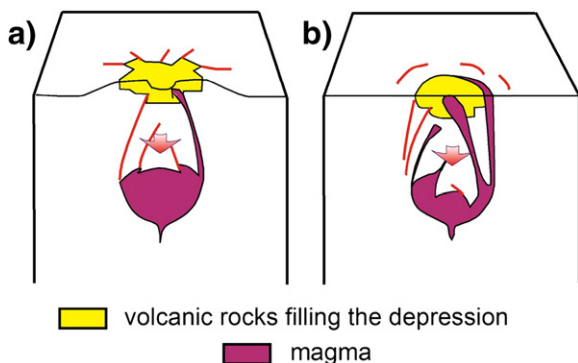

volcanic rocks filling the depression
magma

Fig. 11. Underpressure experiments of Komuro (1987). (a) Inflation+deflation; (b) deflation only (modified after Komuro, 1987).
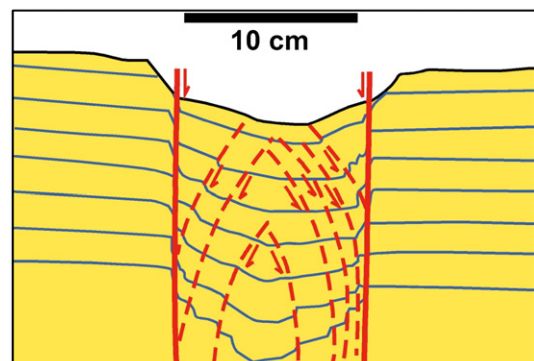

Fig. 12. Underpressure experiments of Martì et al. (1994). Section view of a collapse experiment, characterized by subvertical normal faults and outward dipping reverse faults (modified after Martì et al., 1994).
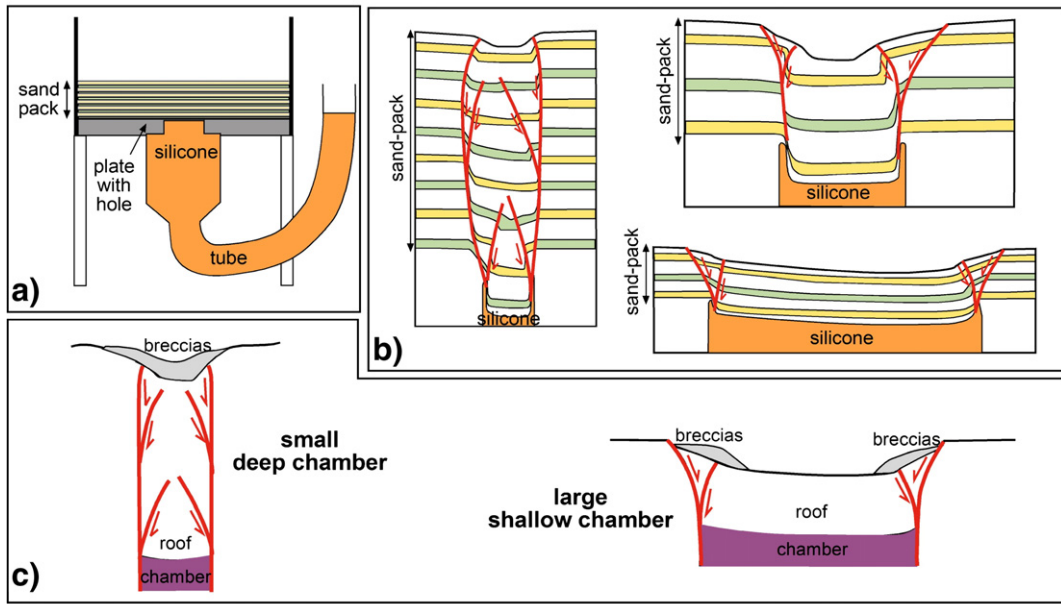
Fig. 13. Underpressure experiments of Roche et al. (2000). (a) Apparatus, section view; (b) section view of three experiments characterized by very different aspect ratios of the chamber roof; (c) final model summarizing the deformation pattern for funnel (small deep chamber) and piston (large shallow chambers) calderas (modified after Roche et al., 2000).
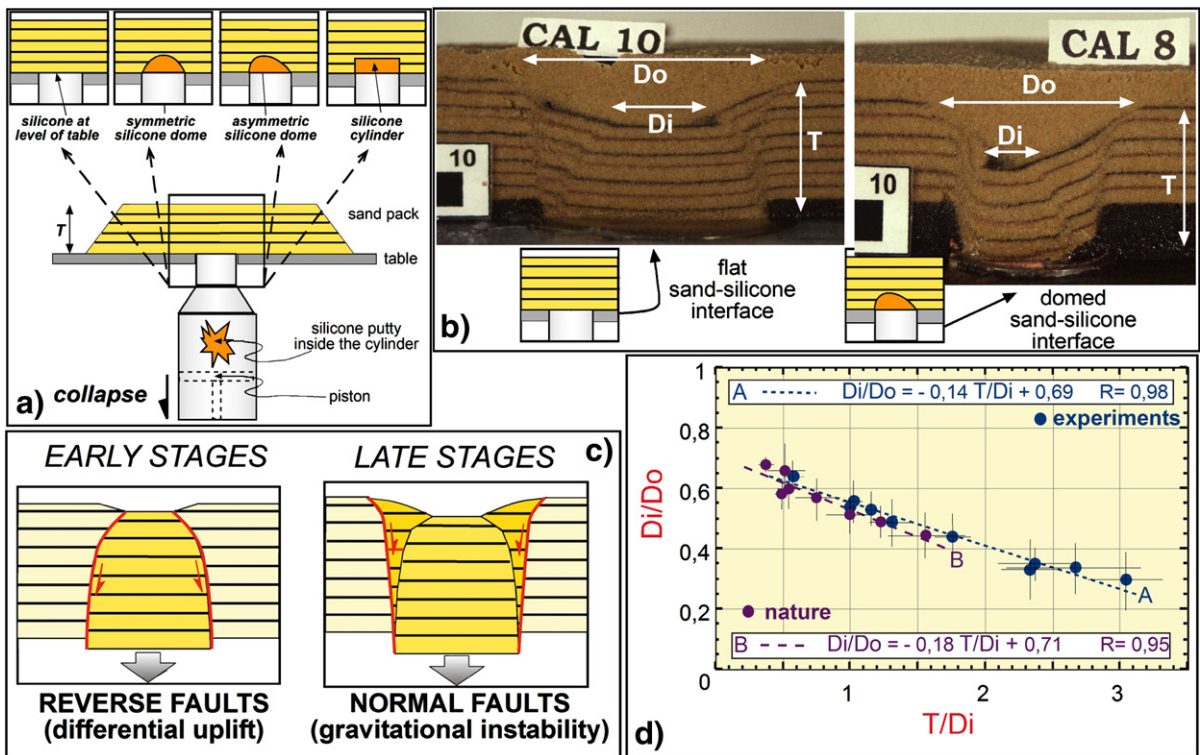

Fig. 14. Underpressure experiments of Acocella et al. (2000). (a) Apparatus; (b) section view of a symmetric and asymmetric collapse and the related imposed conditions; (c) evolution of an experimental caldera (modified after Acocella et al., 2000); (d) consistency of the architecture of nested calderas in nature and experiments (modified after Acocella et al., 2001b).
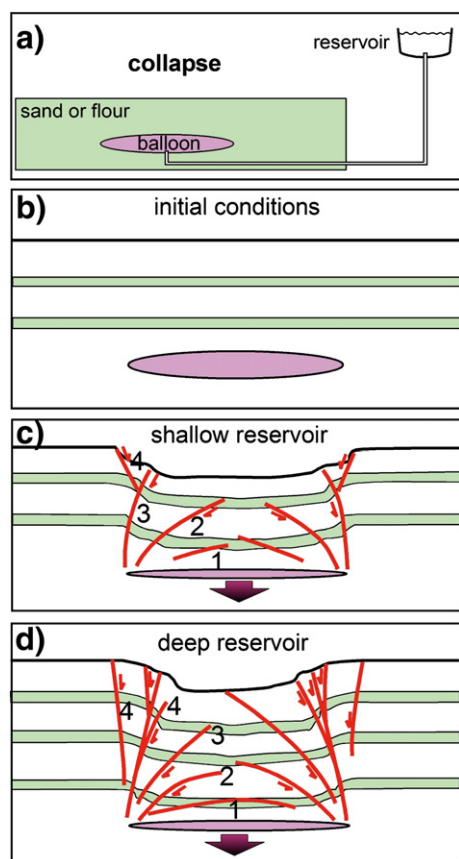
Fig. 15. Underpressure experiments of Walter and Troll (2001). (a) Apparatus; (b) undeformed stage; (c) and (d) examples of final stages of collapse with different aspect ratios of the chamber roof (modified after Walter and Troll, 2001).

inward-dipping normal faults develop. Despite the similarity and consistency with previous models, minor differences exist. These concern the outward incremental growth of the caldera, conversely to what observed with flat roof, where the caldera width is constant (Fig. 16h; Acocella et al., 2000; Roche et al., 2000). Also, both the inner and outer set of faults show a polygonal shape in map view, seldom previously observed (Branney, 1995; Roche et al., 2000). Finally, conversely to Acocella et al. (2001b), trapdoor subsidence is larger where the reservoir is deeper; this results from the larger amount of local subsidence within the reservoir.

4.3.2. Caldera collapse under a regional stress field

Acocella et al. (2004) use the same apparatus and materials as Acocella et al. (2000). Here the sand-pack undergoes "regional extension" (through the lateral sliding of a basal sheet) only before collapse. As the strain rates of caldera collapse ($\varepsilon \sim 10^{-10}$ s^{-1}) are higher than those of

regional tectonics ($\varepsilon \sim 10^{-15}$ s^{-1}), regional extension may be neglected during collapse. Therefore, these experiments simulate only the effect of pre-existing regional normal faults on collapse, not of a coeval regional stress field. The faults are subparallel, mainly with similar dip and plunge (inward dipping at $\sim 60°$), bordering a graben or half-graben. Their main effect is the partial reactivation during the development of the outward dipping reverse ring fault, when the ring fault is near and subparallel (Fig. 17). The reactivation widens the caldera along the direction perpendicular to the normal faults, resulting in an ellipse whose major axis is parallel to the former extension direction. The reactivation may account for the formation of elliptic calderas, with eccentricity >0.8, elongated perpendicular to the rift axis.

Holohan et al. (2005) use the same apparatus as Walter and Troll (2001). The brittle material undergoes regional extension or contraction (through the sliding of a side wall) during collapse (Fig. 18a). Therefore, these models simulate any effect of a regional stress field coeval to collapse. The result is the dip variation of the outward dipping reverse faults (Fig. 18). Under regional extension, along a section parallel to the maximum extension, the reverse faults are subvertical, rather than dipping at $\sim 70°$ (Fig. 18c). The imposed regional extension increases the dip of the maximum direction of compression $\sigma 1$. The opposite occurs under regional compression, where the mean dip of the reverse faults lowers to $\sim 50°$, as due to the increase in the dip of the minimum direction of compression $\sigma 3$ (Fig. 18d). Since these variations are observed only along a direction parallel to $\sigma 3$ (regional extension) or $\sigma 1$ (regional compression), the result is an elliptic caldera, elongated parallel to $\sigma 3$ (during extension) or perpendicular to $\sigma 1$ (during compression). Its minimum eccentricity is ~ 0.8.

4.4. Consistency of the experiments

4.4.1. Collapse related to overpressure conditions

All the experiments of this category share a major similarity, the development of an apical depression as a consequence of doming, regardless of its cause. Its width is much smaller than that of the domed area, whereas its depth is one order of magnitude smaller. This depression, produced by a net uplift in all zones, results from a differential uplift, rather than a collapse and is induced by the tensile stresses developed on the crest of a domed area (Gudmundsson, 1999); in some cases (Martì et al., 1994; Acocella and Mulugeta, 2002), it is bordered by normal faults. It is sometimes accompanied by radial fractures, resulting from the shallow intrusion of the magma analogue, which increases the circumference of the domed
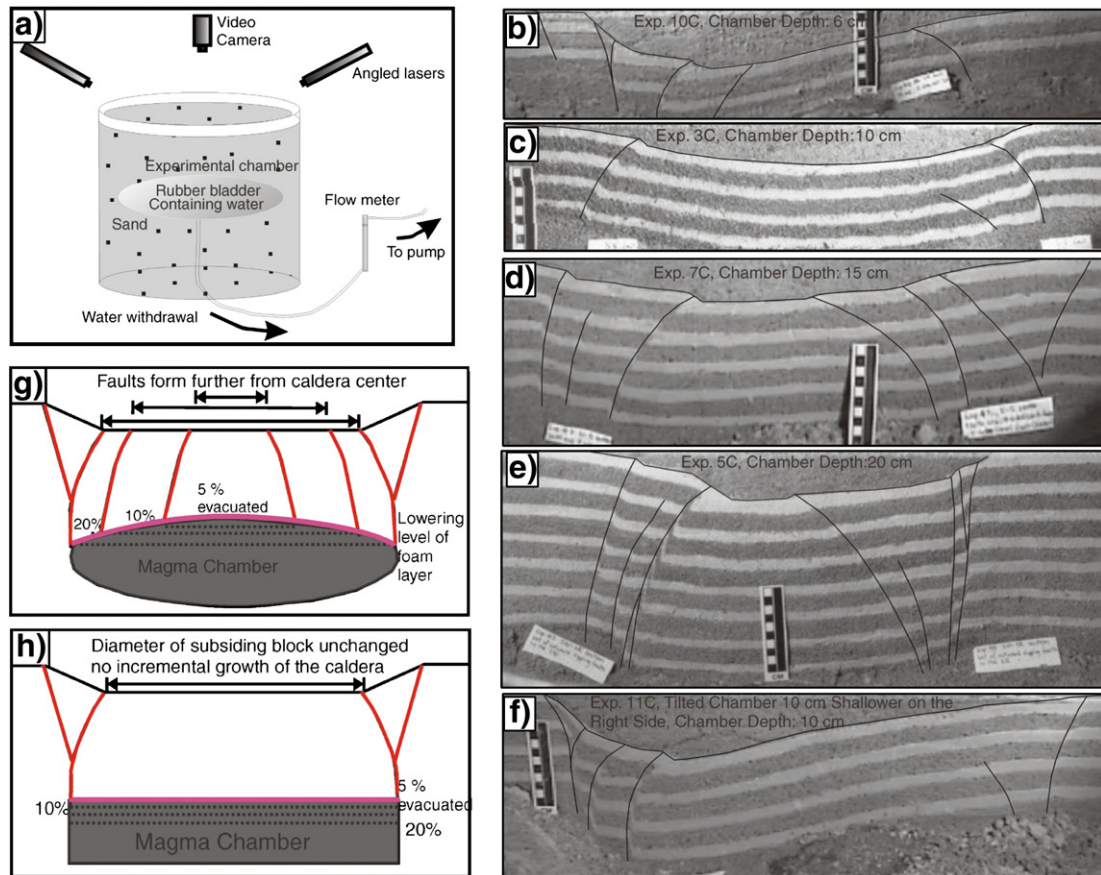
Fig. 16. Underpressure experiments of Kennedy et al. (2004). (a) Apparatus; (b) to (f) examples of different collapses in section view; (g) and (h) modalities of collapse as a consequence of the different shape of the chamber-roof interface (modified after Kennedy et al., 2004).

area (Mandl, 1988). This deformation pattern is in general agreement with those numerical models highlighting the formation of depressions as a consequence of reservoir overpressure (Gudmundsson, 1988; Gudmundsson et al., 1997). The experimental crestal depressions simulate magma-induced depressions in volcanic areas (Komuro et al., 1984; Acocella and Mulugeta, 2002). If we consider calderas as resulting from the rapid withdrawal of the magma chamber, these experimental depressions, induced by doming, should not be considered as calderas. Conversely, if we consider calderas as resulting from an increase in the pressure of the magma chamber (Gudmundsson, 1988), these experimental depressions may be considered equivalent to calderas. However, the experiments show that a significant uplift should occur before developing the depression. This, scaled to nature, should be ≥1 km to induce a depression of a few hundreds of m; larger depressions require uplifts of several km. Tumescence has been commonly considered an important precursor for calderas (Smith and Bailey, 1968; Lipman, 1984). However, evidence of pre-caldera uplift is not

common and usually in the order of 10–100 m (Aizawa et al., 2006, and references therein). Uplifts of a few km, developing summit depressions, have been observed (Acocella, 2000), but are uncommon. Therefore, the experimental uplifts are too large to explain any natural caldera, associated with uplifts 1–2 orders of magnitude smaller. Thus, this category of experiments, not explaining the development of calderas with a subsidence larger than very few hundreds metres, is not adequate to understand both the formation and structure of most natural calderas.

4.4.2. Collapse related to underpressure conditions

Here the most important similarities lie in the development and final deformation pattern of the calderas. Complete collapse consistently gives two ring structures (Fig. 19): an inner outward dipping reverse ring fault and, after a certain slip, an outer inward dipping to subvertical normal ring fault. Each ring may be formed by a single, continuous fault, accommodating all the displacement, or by multiple, closely-spaced concentric ring faults or portions of them. The amount of faults may depend
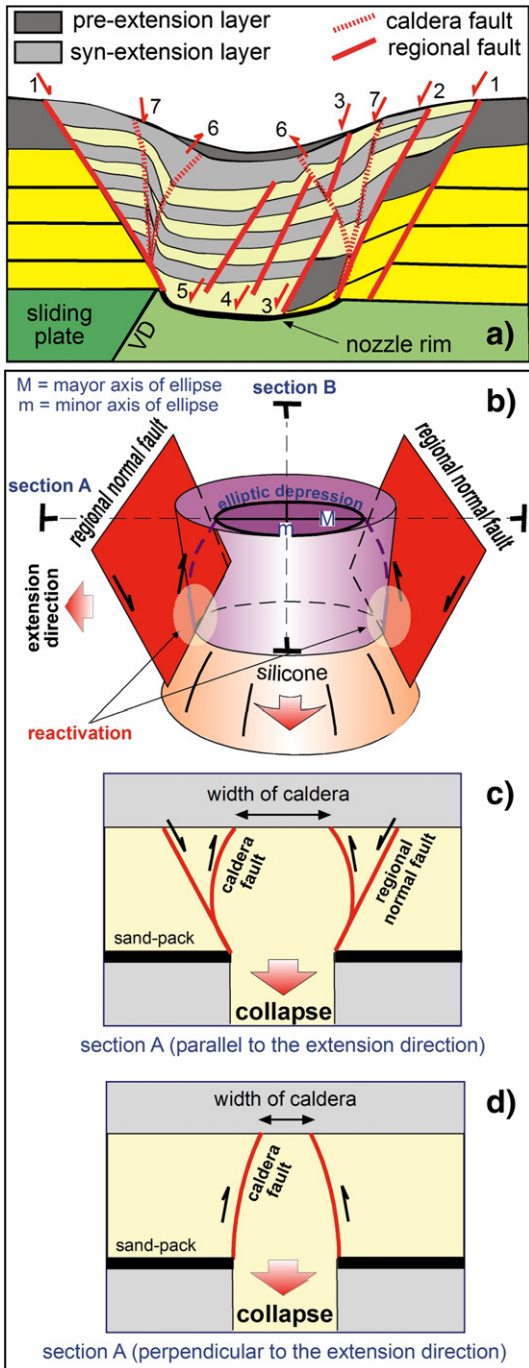
Fig. 17. Experiments with regional stress of Acocella et al. (2004). (a) Section view of an experiment with partial reactivation of the regional faults during collapse; (b) explanation for the ellipticity of the caldera considering the deformation pattern across 2 orthogonal sections (c and d) (modified after Acocella et al., 2004).

et al., 2000; Roche et al., 2000). With a domed shape, strain may accumulate also at the points of maximum curvature of the reservoir (Mandl, 1988), generating additional ring faults (Acocella et al., 2001b). Moreover, if the contraction of the domed-shaped reservoir is not homogeneous and migrates outwards, multiple concentric reverse ring faults form (Martì et al., 1994; Walter and Troll, 2001; Kennedy et al., 2004). Whether consisting of a single fault or a multiple set, the volume delimited by the reverse faults constitutes the sinking piston. The peripheral

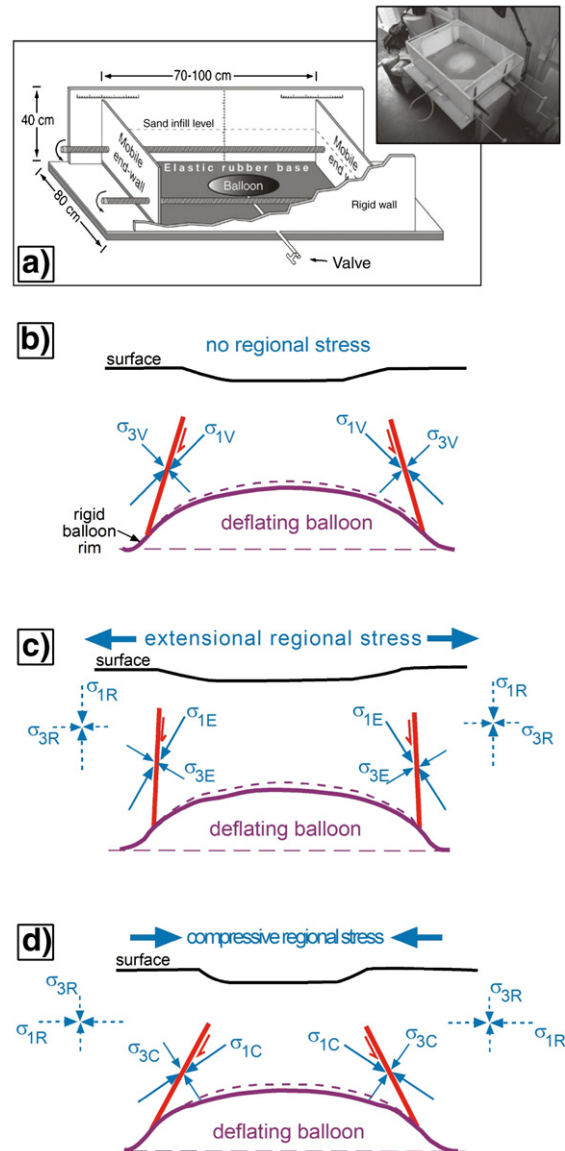Fig. 18. Experiments, with regional stress, of Holohan et al. (2005). (a) Apparatus; section view of the caldera reverse ring faults with neutral (b), extensional (c) and compressional (d) stress field (modified after Holohan et al., 2005).

upon the reservoir shape. With a flat shape, the strain accumulates at the reservoir tips, enhancing the nucleation of a single pair (reverse + normal) of ring faults (Acocella
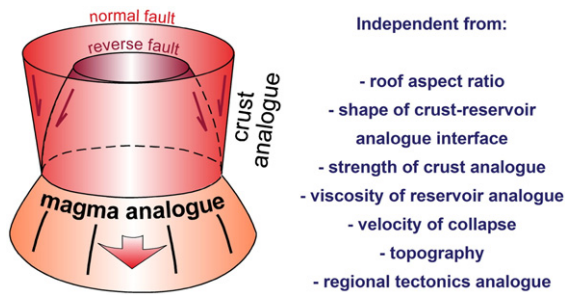
Fig. 19. Model summarizing the final stage of deformation of all the experimental calderas related to underpressure within the reservoir, independently from the listed factors. Outward dipping reverse (first-formed) and inward dipping normal (second-formed) ring faults develop above a magma chamber analogue as a function of the amount of subsidence.

inward dipping normal faults accommodate the gravitational deformation. Multiple concentric ring faults may also form (Walter and Troll, 2001; Kennedy et al., 2004). A consistent deformation pattern has been observed also under a regional stress field (Acocella et al., 2004; Holohan et al., 2005); the only variation lies in the dip of the reverse faults.

Another similarity is the transition from diffuse to localized plastic deformation before and during the development of a ring fault (Fig. 20). Since the collapse is imposed at depth in the experiments, all the ring faults nucleate at the top of the chamber analogue and propagate upwards. In its propagation, the deformation beyond the fault tip is characterized by an inward tilt at the surface. Increased upward propagation of the fault localizes the deformation, forming a scarp replacing the tilt. The inward tilt has been observed in the early stages of all the experiments, suggesting a partially developed collapse, controlled by a limited subsidence.

The architecture of collapse is in part controlled by the roof aspect ratio (Roche et al., 2000). Lower ratios (type A; Section 4.3.1) are associated with one set of reverse and normal faults, while higher ratios (type B; Section 4.3.1) with multiple sets of reverse faults and eventually, a set of normal faults on top (Fig. 13). However, the overall deformation pattern is consistent in both cases. In fact, in type B experiments, multiple reverse faults are required to propagate the collapse upwards in a thicker crust analogue. Normal faults, as resulting from the gravitational collapse of the wedges above the upper reverse ring fault at surface, form only if the displacement along this upper fault reaches a certain amount of slip. The same is observed with type A experiments. Therefore, independently from the roof aspect ratio, all the collapses may display one or more set of reverse faults; if the displacement on the upper ring fault at surface reaches a certain threshold, a normal ring fault may also form.

In synthesis, all the experimental underpressure collapses generate outward dipping reverse ring faults and peripheral inward dipping normal ring faults, both replacing former tilts. This behaviour is observed with different apparatus and materials (sand, flour or clay as brittle crust analogue and air, water and silicone as magma analogue), scaling (times, strain rates and lengths), topography (with or without volcanic edifices, with various slope dips), stress fields (neutral, compressional, extensional) and caldera elongation. The same structures were obtained in experiments investigating differential uplift (Sanford, 1959) and the depletion of reservoirs (Odonne et al., 1999). Such a general consistency indicates that the experimental deformation pattern during collapse is independent from the strength of the brittle crust analogues, the viscosity of the magma analogue, the duration and size of the experiment and the presence of a regional stress field or the load of any edifice (Fig. 19). This indicates a precise structural behaviour in accommodating the room problem during collapse, inferring a wide applicability of the analogue results.

Despite this general agreement, minor discrepancies do exist. Possibly, the most relevant concerns trapdoor
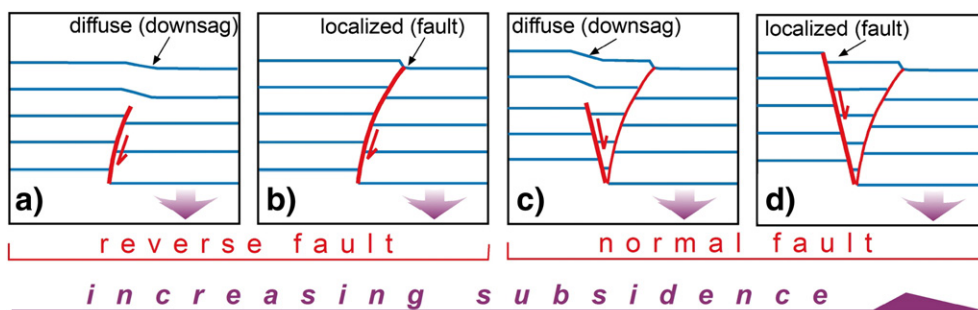

Fig. 20. Diffuse (inward tilt at surface; a and c) and localized (scarp at surface; b and d) deformation due to the upward propagation of the reverse (a and b) and normal (c and d) ring faults at the periphery of the caldera during progressive subsidence.

collapses, common in Roche et al. (2000), Walter and Troll (2001) and Kennedy et al. (2004), and rare in Acocella et al. (2000). Some of the obtained trapdoor structures were expected, due to the imposed conditions, as the shape of the chamber analogue (Acocella et al., 2001b) or the distribution of the roof load (Kennedy et al., 2004). Other trapdoors were unexpected, and may have occurred due to heterogeneities difficult to control *a-priori* (Roche et al., 2000). Moreover, in Acocella et al. (2000), the most subsided part of the trapdoor is above the top of the asymmetric domed reservoir. Conversely, in Kennedy et al. (2004), the most subsided part is above the most depressed area of the reservoir. This apparent discrepancy can be explained by the fact that, when the subsidence is homogeneous, the faults form along the points of maximum curvature of the top of the reservoir, located in its most uplifted part. As a consequence, the maximum subsidence is observed above the most uplifted part of the reservoir (Acocella et al., 2001b). Conversely, with a differential subsidence within the reservoir (as when deflating a balloon), the deepest area at surface coincides with the most emptied area in the reservoir (Kennedy et al., 2004).

4.5. Towards a consistent experimental model

The consistency among the experiments simulating underpressure, under different boundary conditions, allows a comprehensive experimental model to be proposed. This is summarized through four main stages, representing discrete moments within an evolutionary continuum controlled by the amount of subsidence (Fig. 21).

Stage 1 is characterized by a downsag depression, with inward tilted margins (surface accommodation of the buried reverse fault) at the surface (Fig. 21a). This occurs with a subsidence of very few mm (in a caldera a few cm wide), corresponding to 10^1–10^2 m in nature. At Stage 2, the reverse fault reaches surface, replacing the downsag. This occurs with a subsidence of several mm, corresponding to $\sim 10^2$ m in nature. The structural boundary is completely defined, exhibiting a clear rim or scarp, above the reverse fault. While the reverse fault is always outward dipping, the rim above, due to rapid decay of the overhanging reverse fault scarp, is subvertical or inward dipping. Additional reverse ring faults may be present, accordingly with the mode of outward incremental growth (Kennedy et al., 2004). At this stage, the basic structure of the experimental caldera resembles a piston-type (lower roof aspect ratios) or funnel-type (higher aspect ratios) (Fig. 21b; Roche et al., 2000). Stage 3 results from further increase in subsidence, ~ 1 cm, corresponding to ~ 1 km in nature. This develops a peripheral inward tilt or

downsag, as the surface accommodation of the buried normal fault (Fig. 21c). Stage 4 results from subsidence of 1 cm or more, corresponding to ≥ 1 km in nature. This develops an outer normal ring fault, replacing the former tilt, forming an additional scarp. As slip along the reverse fault still continues, the collapse structure consists of a pair of nested calderas, given by two concentric ring faults (Fig. 21d). No variation in the deformation pattern is observed increasing the subsidence.

The estimates of the amount of collapse required to reach a certain stage vary depending upon the diameter of the caldera (d) and thickness of the brittle material (t). The variation of the subsidence s with d and t, based on the experiments of Acocella et al. (2000), is shown in Fig. 22. Keeping t constant ($t=5$ cm), the subsidence required to reach any stage in Fig. 22a increases with d. This suggests that the larger the caldera diameter, the larger the subsidence accommodated at stages 1 and 3. As a result, faulting at stages 2 and 4 also occurs for larger amounts of subsidence. Therefore, the above-given estimates for the subsidence required to reach a certain collapse stage are purely indicative, as they refer to a caldera a few cm wide, and should be considered significantly dependent from the diameter of the natural caldera. Keeping d constant ($d=5$ cm), a direct proportion between the subsidence s and t is observed for the 4 stages (Fig. 22b). This implies that a thicker sand-pack requires a higher subsidence to reach a certain stage. As the faults nucleate at the bottom of the sand-pack and propagate upwards, this behaviour results from the fact that thicker sand packs require a greater displacement to be completely faulted through. Because the duration of the experiment controls the amount of subsidence, a higher subsidence is necessary to reach the same stage in a thicker sand-pack.

4.6. Analogue vs. numerical models: comparison of their results

As anticipated, the numerical models give controversial indications on the structure and development of calderas, depending on the imposed conditions and assumptions. The results of Kusumoto and Takemura (2003) are in agreement with the underpressure analogue experiments, developing a similar deformation pattern. Burov and Guillou-Frottier (1999) also develop consistent results, generating upward propagating subvertical (the poor resolution hinders a precise estimate of the dip direction) to inward dipping faults. These similarities suggests that the observed deformation pattern is not limited to the conditions imposed in the analogue models, but may in principle be applied to any modelling technique.
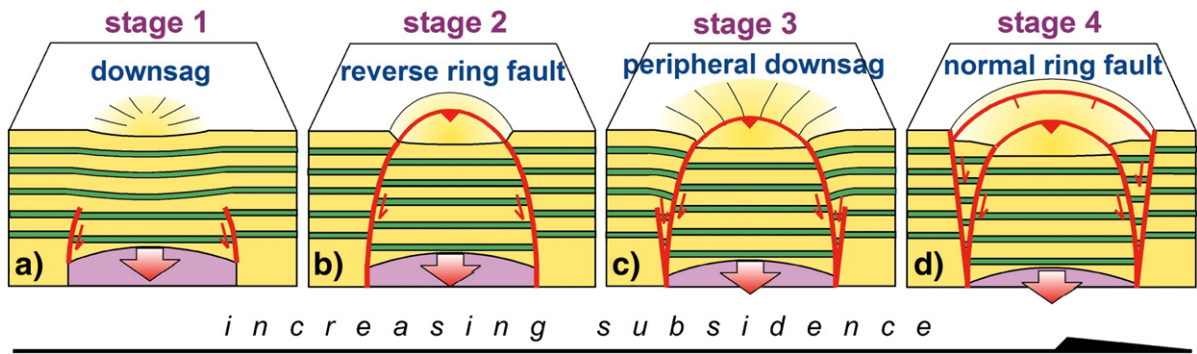
Fig. 21. Schematic representation of the four stages of evolution of caldera collapse, obtained in all the underpressure experiments, as a function of the amount of subsidence.

Other numerical models (Gudmundsson et al., 1997; Gudmundsson, 1998b; Gray and Monaghan, 2004; Pinel and Jaupart, 2005) are in partial or total disagreement with the analogue models. Common features with the overpressure experiments are the formation of normal faults bordering a depression during doming (Gudmundsson et al., 1997; Gudmundsson, 1998b). However, substantially different features with the underpressure experiments are the normal faults (Burov and Guillou-Frottier, 1999; Folch and Martì, 2004) propagating downward during collapse (Gudmundsson et al., 1997; Gudmundsson, 1998b; Gray and Monaghan, 2004; Pinel and Jaupart, 2005). These discrepancies may lie in the conditions imposed in these models: a) a cavity undergoing only changes; b) the elastic rheology of the simulated crust; c) the frequent (not common to all the models) use of sill-like geometries. Condition a) may hinder the simulation of significant volume changes in the chamber, essential to develop large calderas (Cole et al., 2005 and references therein); interestingly, those elastic models considering volume changes (Kusumoto and Takemura, 2003) are consistent with the experiments. Condition b) may hinder the possibility to appreciate discontinuous solutions, and therefore the precise fault pattern. Condition c) in the elastic models may enhance flexuring at surface during collapse, as sill-like reservoirs are associated with lower roof aspect ratios with higher flexural response (Turcotte and Schubert, 1982). Therefore, tensile stresses (and thus downward propagating normal faults) on the upper flexure are enhanced (Folch and Marti, 2004).

In synthesis, the results of the numerical models do not permit a straightforward comparison with the analogue experiments. In general, their discrepancies with the experiments may be explained by the different geometric (shape of reservoir), kinematic (pressure variations in the reservoir) or rheological (elastic behaviour) conditions. Moreover, the controversial results of the numerical models, due to their boundary conditions, are not observed in the analogue models. This suggests that the analogue
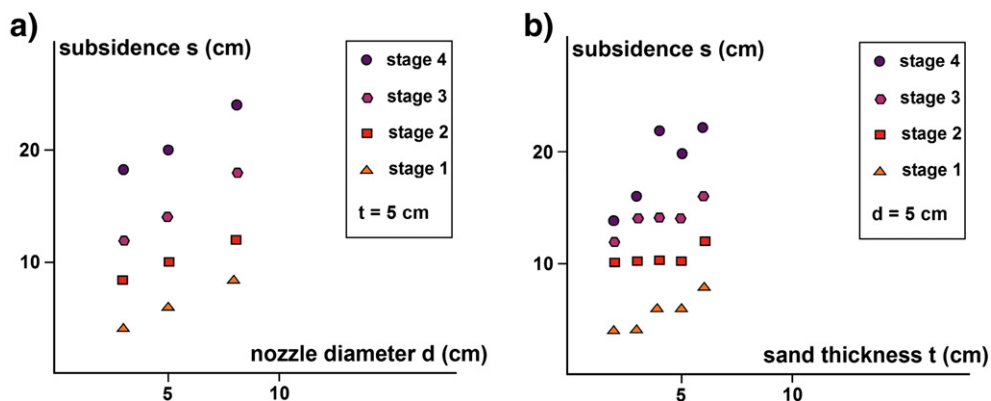

Fig. 22. Variation in subsidence of experimental calderas with (a) nozzle diameter and (b) thickness of the sand pack. Data taken from Acocella et al. (2000).

experiments may be efficaciously used to understand natural calderas.

5. Comparison of analogue experiments with observed calderas

The consistency among the underpressure experiments simulating calderas, regardless of their boundary conditions, is now used for a comprehensive comparison to natural calderas, taking into account the available geological and geophysical data.

5.1. Qualitative features

The main structural features of the experiments are the downsags (stages 1 and 3) and ring faults (stages 2 and 4), both visible at well-studied calderas. The sagged floor may be the only structure accommodating subsidence, as at Bracciano (Italy; Di Filippo, 1993) or Buckhorn (Texas; Henry and Price, 1984), or may be accompanied by a ring structure within, as at Bolsena (Italy) (Fig. 23; Walker, 1984; Nappi et al., 1991), Rotorua and Reporoa (New Zealand; Spinks et al., 2005, and references therein). Many downsags have later turned into ring faults, as Sabaloka (Sudan; Almond, 1977), Ishizuchi (Japan; Yoshida, 1984) and Grizzly Peak (Colorado; Fridrich and Mahood, 1984; Fridrich et al., 1991), consistent with the experimental evolution. While the presence of a ring fault at the surface may be highlighted by the caldera structural rim, its location at depth is more uncertain. This has generated a debate over the fault's nature, variously described as normal inward dipping, reverse outward dipping or vertical (Kennedy and Styx, 2003). Despite the common expectation that calderas are bordered by normal faults (Newhall and Dzurisin, 1988, and references therein), there is widespread, scale-invariant evidence for outward dipping reverse faults bordering collapses. At the m scale, ice-melt collapse pits and mining subsidence structures consistently show inward tilted margins at surface, associated with extension fractures, above outward dipping reverse faults (Fig. 24a; Branney, 1995, and references therein; Branney and Gilbert, 1995). Even though not generated by magma emplacement, these structures are remarkably consistent with those of experimental calderas, providing an important scale connection, from the laboratory to nature. At the 10–100 m scale, subcircular collapses and pit craters are bordered by outward dipping reverse faults, as at Taupo Volcanic Zone (New Zealand), Masaya volcano (Nicaragua) and Erta Ale, Afar, Ethiopia) (Fig. 24b to d; Branney, 1995; Rymer et al., 1998; Roche et al., 2001; Acocella, 2006a). At the km-scale, outward dipping reverse faults formed

during the early collapse at Miyakejima in 2000, possibly the most significant collapse (with subsidence of several hundreds of m and fracturing) observed so far (Fig. 3; Geshi et al., 2002). At larger scales (several km), outward dipping ring faults border Rabaul (Fig. 4; Mori and Mckee, 1987; Saunders, 2001), Ishizuchi (where they may have developed before the outer ring system; Yoshida, 1984; Yoshida, pers. comm.), Colli Albani (Italy; Giordano et al., 2006), Sierra Negra, (Galapagos; Jonsson et al., 2005) and Misema (Canada; Mueller, pers. comm.). Outward dipping faults also accompanied the collapse of the chamber roof during the Pinatubo 1991 and Mt St Helens 1980 eruptions (Fig. 4; Scandone and Malone 1985; Mori et al., 1996), even though no caldera formed at the surface. Peripheral normal ring faults may be present as well, as at Miyakejima (Fig. 3; Geshi et al., 2002) or Rabaul (Saunders, 2001), forming pairs of concentric ring faults, as in stage 4 experiments. Such nested pairs of concentric calderas are common, as at Campi Flegrei, Latera, Pantelleria (Italy), Tavua (Fiji), Batur (Indonesia), Fantale (Ethiopia), Taupo (New Zealand), Suswa (Kenya), Guayabo (Costa Rica), Daisetsu (Japan), Karkar and Rabaul (Papua New Guinea) (Fig. 25; Acocella et al., 2001b, and references therein; Acocella et al., 2002). Differential collapse of these structures may result in trapdoors, observed in the experiments and in natural calderas, as at Grizzly Peak (Colorado; Fridrich et al., 1991), Bolsena (Fig. 23), Latera (Italy; Nappi et al., 1991), Kumano (Japan; Miura, 2005) and Coromandel Peninsula (New Zealand; Smith et al., 2006). These show a differential subsidence, accommodated by ring faults (deeper part) and flexures (shallower part).

The progression of experimental structural features is also commonly found at several well-studied calderas (as Sabaloka, Ishizuchi, Grizzly Peak, Miyakejima, Bolsena, Colli Albani and Guayabo). At many calderas, these structural features may easily overlap. This may occur with advanced subsidence, when older structures remain preserved, or with asymmetric collapse, developing structures apparently corresponding to different collapse stages along the caldera.

These consistencies between models and nature suggest that the structure of many natural calderas can be interpreted from underpressure experiments. Moreover, the surface structure of experimental calderas corresponds to precise structures at depth, whose evolution has been summarized in the above-mentioned four stages. Therefore, the analogue models may provide an invaluable key to infer the subsurface structure of calderas from their surface structure. In fact, despite possible overlaps of structural features within a caldera, it is in principle
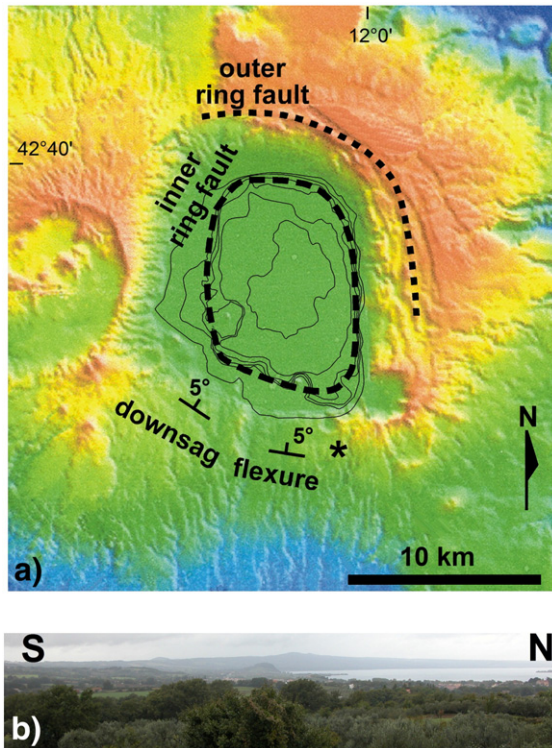
Fig. 23. (a) Simplified structure of Bolsena caldera, Italy, consisting of an inner ring structure, buried within the lake (spacing of lake contours = 25 m) and a subsequently formed outer set of ring structures, in its northern part; to the south, this is replaced by an inward tilt, forming a downsagged caldera margin, also visible in the photo (b) (modified after Nappi et al., 1991; Simei et al., 2006). Asterisk in (a) shows location of picture in (b).

possible to recognize the evolutionary stage of a caldera accordingly with its overall surface structure, provided that this is known. Several calderas, with a constrained surface structure, may be appropriate examples of the 4 experimental stages (Fig. 26). An example of stage 1 caldera is Bracciano, Italy, with a diameter of ∼12 km, subsidence of ∼300 m and inward tilted slopes, without evident faulting (Fig. 26a; Di Filippo, 1993; Barberi et al., 1994). Despite post-caldera volcanic activity, the architecture of Bracciano resembles a downsag. An example of a stage 2 caldera is Erta Ale, Ethiopia, with a diameter of ∼1 km and bordered by a subvertical scarp, few tens of m high, overlying a ring fault (Fig. 26b; Acocella, 2006a). Other examples of a stage 2 caldera include Kilauea and Mauna Loa, both characterized by a fault-controlled rim, even though additional peripheral buried ring faults may be present (Newhall and Dzurisin, 1988). Here the decay of the overhanging reverse fault scarp develops subvertical to inward dipping rims towards the outer border. Therefore, the structural boundary lies in an inner position

with regard to the morphological rim. An example of a stage 3 caldera is Rotorua, New Zealand, ∼20 km wide, with a subsidence of ∼1 km (Fig. 26c). Despite minor

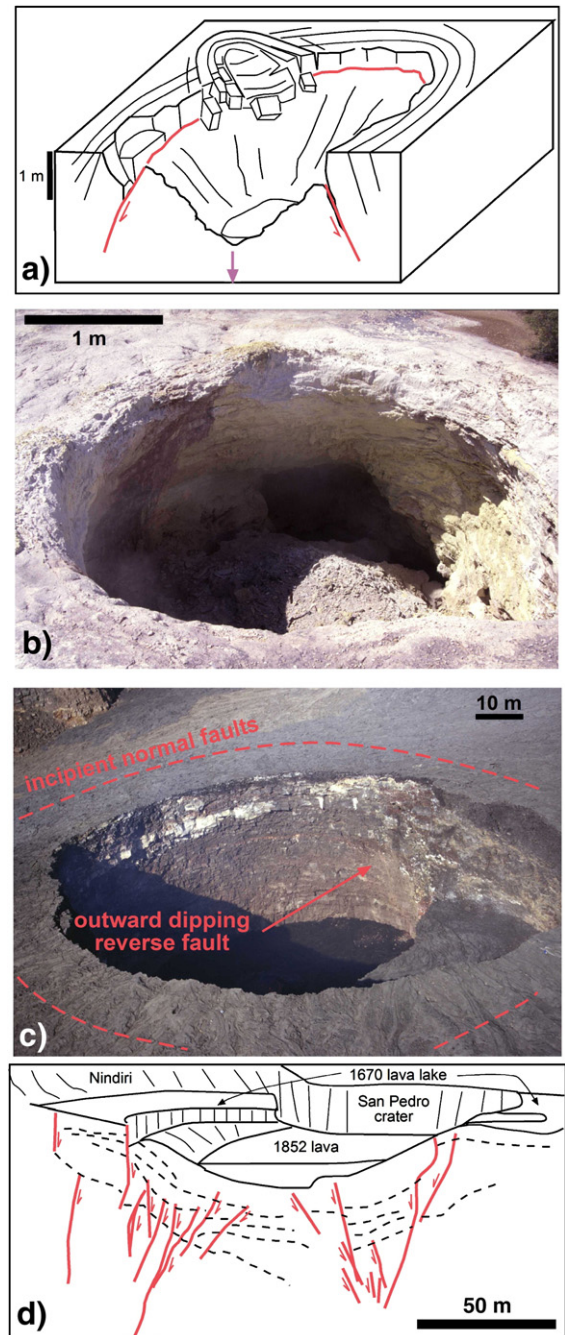Fig. 24. Natural examples of high angle outward dipping reverse ring faults bordering collapses and pit craters at various scales, from m to hundreds of m. (a) structure of ice-melt collapse pits in unconsolidated sediments (after Branney, 1995); (b) collapsed structure at Taupo Volcanic Zone, New Zealand, (c) Erta Ale, Ethiopia; (d) Masaya, Nicaragua (scale is approximate; modified after Roche et al., 2001).
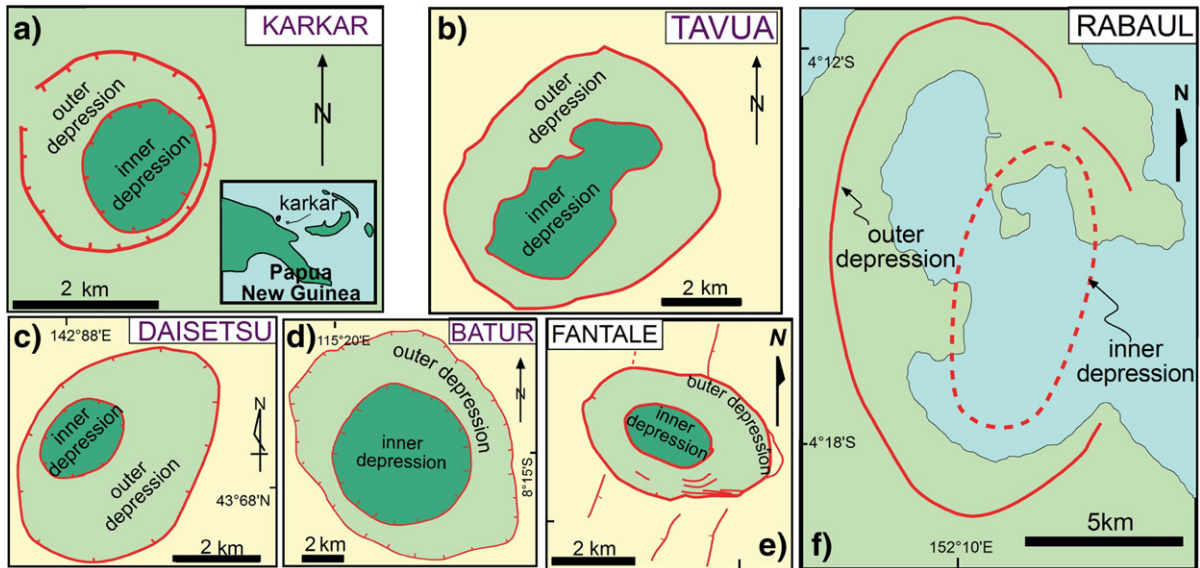
Fig. 25. Examples of pairs of nested calderas with similar elongation direction and eccentricity, at (a) Karkar (Papua New Guinea), (b) Tavua (Fiji), (c) Daisetsu (Japan), (d) Batur (Indonesia), (e) Fantale (Ethiopia) and (f) Rabaul (Papua New Guinea) (modified after Acocella et al., 2001b, 2002).

faults, its overall structure resembles a downsag, with inward-tilted slopes and a central ring structure, bordering a subcircular depression (Milner et al., 2002; Spinks et al., 2005). An example of an advanced stage 3 caldera is Bolsena, Italy (Fig. 23). This, like Rotorua, has an outer downsag (~17 km wide) bordering an inner depression, accommodating a subsidence of ~1000 m (Walker, 1984; Barberi et al., 1994; Simei et al., 2006). The main difference is that ~1/3 of the downsag (NE portion; Fig. 23) is replaced by a ring fault, due to locally increased subsidence (Simei et al., 2006). An example of a stage 4 caldera is Campi Flegrei, Italy, ~16 km wide, with a subsidence of ~2 km, forming two nested depressions bordered by concentric ring faults (Fig. 26d; Barberi et al., 1991; Orsi et al., 1996; Florio et al., 1999; Acocella and Faccenna, 2007). Additional examples include Latera (Italy; Fig. 26d; Nappi et al., 1991), Guayabo (Costa Rica; Hallinan, 1993; Hallinan and Brown, 1995) and White-horse (USA; Rytuba and McKee, 1984).

The experiments suggest that the concentric pairs of nested calderas are related to the same eruptive episode (Martì et al., 1994; Acocella et al., 2001b), not necessarily to two distinct eruptions (e.g. Newhall and Dzurisin, 1988, and references therein). One can discriminate between the two possibilities only constraining the timing of development of the two collapses. In fact, surface data can only indicate that the outer caldera is older, as otherwise the inner would have been covered by the activity of the outer, as Campi Flegrei, Latera, Tavua (Orsi et al., 1996; Capaccioni et al., 1987; Setterfield et al., 1991). Interestingly, subsurface data and sections at these

calderas indicate that the inner depression coincides with an older collapse, later reactivated (Fig. 26d, the fault dips of are approximate; modified after Nappi et al., 1991; Orsi et al., 1996). The different thickness of the syn-collapse deposits indicates that the inner depression formed before the outer one, while the syn-collapse deposits in both depressions suggest their interaction during the same collapse event. These features are in close agreement with the evolution of the experiments. Therefore, surface geology alone is not sufficient to evaluate the relative timing of development of the depressions and to define whether a pair of nested calderas is consistent with stage 4 or results from two distinct collapses.

Several large natural calderas, with a low roof aspect ratio (<0.5) and significant subsidence (>2000 m), have only one major ring fault visible, as Long Valley (Carle, 1988), Valles (Self et al., 1986), La Garita, Creede, Yellowstone (Smith and Braile, 1994, and references therein; Lipman, 1997, 2003), USA, and Okueyama (Japan; Aramaki et al., 1977). They are interpreted as being bordered by two ring faults lying next to each other. Their proximity makes it difficult to resolve each structure separately, so at the caldera scale it appears as a single ring system. A similar deformation pattern is shown in experiments with $A<0.5$ and significant subsidence (Fig. 13b; Roche et al., 2000).

5.2. Quantitative features

This section constrains, in a more quantitative way, the consistency between all the experimental sets and nature.
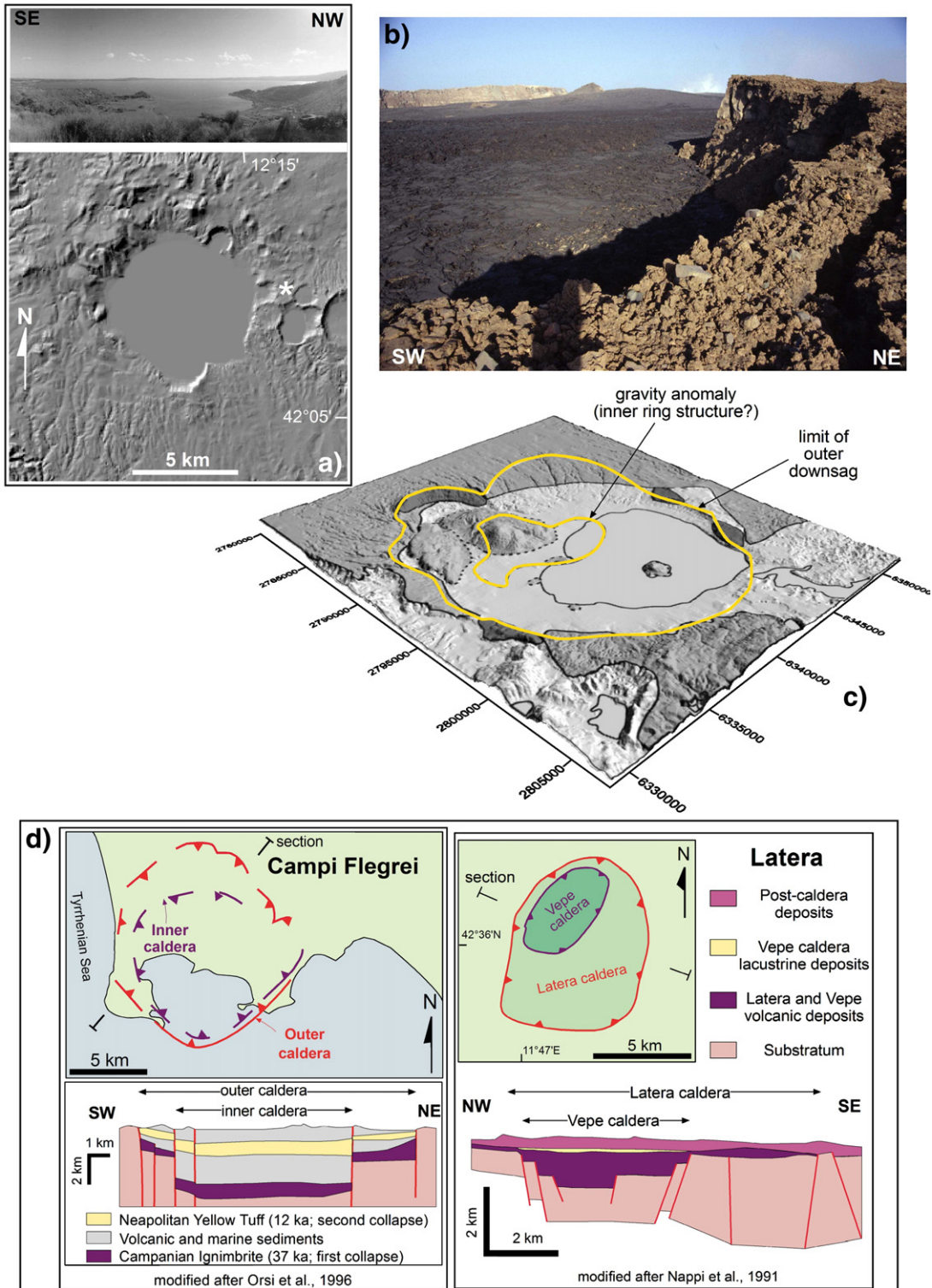
Fig. 26. Natural examples whose overall structure corresponds to the four main stages of experimental collapses: (a) Stage 1: Bracciano, Italy (asterisk in the DEM shows the location of the point of view of picture above); (b) Stage 2: Erta Ale, Afar; (c) Stage 3: Rotorua, New Zealand (kindly provided by Karl Spinks); (d) Stage 4: Latera and Campi Flegrei, Italy.

Table 3
Most of the best-known natural calderas, whose diameter d, collapse s and volume of erupted magma are evaluated (see related references)

Caldera	Diameter (km)	Collapse (m)	Erupted magma (km³)	Stage	Reference
Buckhorn	23±5	400±100	220±20	1	Henry and Price, (1984)
Bracciano	12±1	300±100	(20)	1	Di Filippo (1993)
Denham	5±1	>300	12±4	2	Worthington et al. (1999)
Erta Ale	1±0.5	70±20	<1	2	Acocella (2006a)
Kilauea	4±0.5	150±50	2±0.5	2	Newhall and Dzurisin (1988)
Mauna Loa	4±1	150±50	2±0.5	2	Newhall and Dzurisin (1988)
Gariboldi	5±0.5	>200		2	Acocella et al. (2002)
Roccamonfina	6±1	400±300	130±20	2	De Rita and Giordano (1996)
Darwin	5.5±0.1	200±100	4±1	2	Munro and Rowland (1996)
Alcedo	6.8±0.7	300±100	8±2	2	Munro and Rowland (1996)
Sierra Negra	8±1	200±100	5±1	2	Munro and Rowland (1996)
Krafla	9±0.5	370±100		2	Gudmundsson and Nilsen (2006)
Askja	9±0.5	180±50	(11)	2	Gudmundsson and Nilsen (2006)
Oskjuvatn	4±0.5	250±50	(3)	2	Gudmundsson and Nilsen (2006)
Vico	6.5±1	300±200	60±20	2	Sollevanti (1983)
Glencoe	10±3	>700	63±10	3	Moore and Kokelaar (1998)
Rotorua	20±2	1200±400	150±30	3	Milner et al. (2002)
Reporoa	12±1	1000±400	100±30	3	Spinks et al. (2005)
Bolsena	17±1	1000±300	(147)	3	Barberi et al. (1994)
Pueblo	18±7	1500±300	>300	3	Rytuba and McKee (1984)
Latera	8±1	1500±200	(45)	4	Barberi et al. (1994)
Campi Flegrei	16±2	2000±200	200±30	4	Orsi et al. (1996)
Guayabo	8±3	1000±200	(28)±10	4	Hallinan (1993)
Long Valley	24±6	2600±300	850±200	4	Carle (1988)
Batur	12±1	800±500		4	Newhall and Dzurisin (1988)
Bromo-Tengger	9±2	>1000	(280)	4	Newhall and Dzurisin (1988)
Taupo	22±6	3000±300	480±120	4	Davy and Caldwell (1998)
Valles	22±2	2000±500	1100±100	4	Self and Wolff (2005)
Fantale	4±1	>400		4	Acocella et al. (2002)
Whitehorse	15±1	>800	50±10	4	Rytuba and McKee (1984)
Miyakejima	1.6±0.3	500±100	<1	4	Geshi et al. (2002)
Suswa	12±1	800±300	35±5	4	Skilling (1993)
Okueyama	25±3	2000±1000	(250)	4	Aramaki et al. (1977)
La Garita	40±10	4000±500	2500±500	4	Lipman (1997)
Creede	20±2	4000±500	205	4	Lipman (1997)
Wolf	5.8±0.7	700±200	9±2	4	Munro and Rowland (1996)
Tavua	6.5±1	2000±500	(33)±10	4	Setterfield et al. (1991)
Cerro Azul	3.8±0.5	500±100	3±1	4	Munro and Rowland (1996)
Fernandina	5.5±1	1100±200	12±3	4	Munro and Rowland (1996)
Rabaul	12±2	3000±1000	(300)	4	Bai and Greenlangh (2005)
Hakone	9±1	1800±300	105±20	4	Kuno et al. (1970)
Cotepeque	8.5±1.5	>600	(20)	4	Newhall and Dzurisin (1988)
Aira	20±2	1700±300	300±50	4	Aramaki (1984)
Karthala	3±1	400±100	3±1	4	Mouginis-Mark and Rowland (2001)
Ishizuchi	7.5±0.5	>1000	(60)±20	4	Yoshida (1984)
Nindiri	0.4±0.1	100	<1	4	Rymer et al. (1998)

The corresponding evolutionary stage is assigned from the comparison between the structure of the calderas and the analogue models.

A list of 46 calderas, whose surface structure is con-strained by geology and geophysics, is shown in Table 3 and includes the estimated mean diameter, amount of subsidence and DRE volume of erupted magma (numbers in bracket indicate this is unknown and is replaced by the estimated volume of the caldera) associated with the calderas. The possible evolutionary stage of a caldera is suggested, based primarily on the type of the surface and, when known, subsurface structural features (downsags, ring faults). Calderas without a sufficient knowledge of their surface and subsurface structure have not been included. Table 3 is the first quantitative attempt to understand and classify coherently most of the best-known calderas. The mean diameter, subsidence and

erupted volumes of the calderas in Table 3 are shown by Fig. 27. The calderas appear largely clustered accordingly with the 4 experimental stages, suggesting an agreement between their diameter/subsidence ratios and evolutionary stage. Stage 1 calderas cluster to the lower right of the diagram, with low subsidence and medium to high values of diameter. Stage 2 calderas, above, have moderate subsidence and low to medium diameter. Stage 3 calderas, above, have medium subsidence and diameter, whereas stage 4 calderas, further above, have larger subsidence and low to high diameters. Most of these 4 caldera types cluster within areas approximately bordered by dashed lines, with different d/s (diameter/subsidence) values. These are a schematic visualization of broad transitional zones among caldera stages along a continuum, and not sharp boundaries. Stage 1 calderas are characterized by d/s>40, stage 2 by 18<d/s<40, stage 3 by 14<d/s<18 and stage 4 by d/s<14. The few exceptions (as Reporoa, Roccamonfina, Askja, Whitehorse) are always located

very near to the boundary of their ideal domain and are not considered significant. Rather, these 4 consecutive domains confirm that the development of natural calderas follows a progression, as observed in the experiments. This progression is, for a given caldera diameter, primarily controlled by the amount of subsidence. However, wider calderas have larger tilted margins, accommodating larger amounts of collapses through downsags. This explains the leftward dip of the dashed lines in Fig. 27. The consistent distribution of data in Fig. 27 suggests that, in principle, the d/s ratio may permit to evaluate the overall structure and evolutionary stage of a caldera even when its surface structure is poorly known.

The erupted volumes show a broad correlation with the evolutionary stage (Fig. 27). Stage 4 calderas are usually associated with the largest volumes, while most of the stage 2 calderas are associated with the smallest volumes. This suggests that, in general, more structurally-evolved calderas are related to larger erupted volumes and less
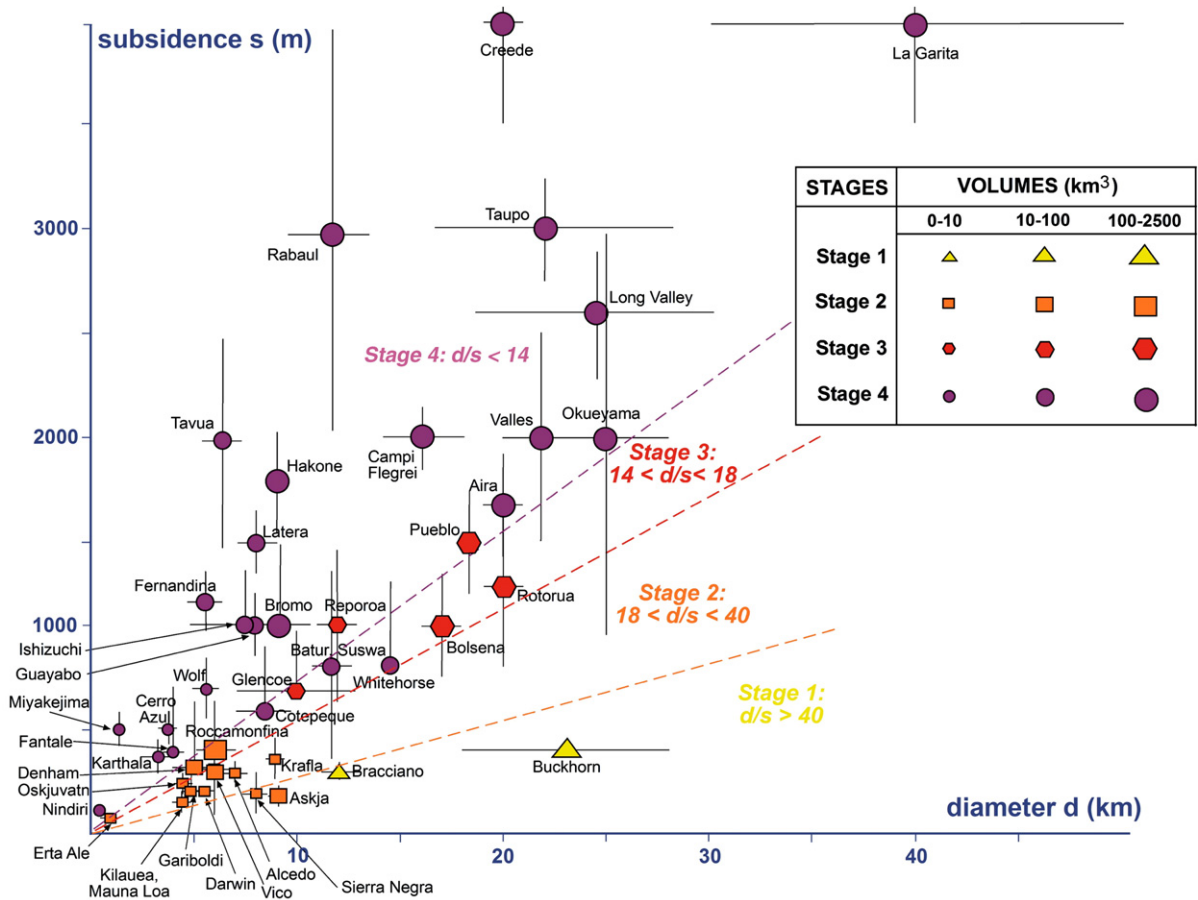

Fig. 27. Variation of subsidence (s) with the diameter (d) of the natural calderas listed in Table 3. The calderas are classified accordingly with the 4 experimental stages (Fig. 21). Dashed lines define specific d/s ratios for each caldera stage. The size of the symbols is proportional to the DRE volume of erupted magma during the formation of the caldera (inset). See text for further details.

evolved calderas to smaller volumes. However, notable exceptions do exist. Miyakejima (stage 4) is related to the removal of only ~1 km^3 of magma in 2000 (Fig. 27), possibly because of its limited diameter, while Buckhorn (stage 1) extruded more than 200 km^3 of magma (Fig. 27), possibly because of its large diameter. Despite the general proportion, the amount of extruded magma associated with a certain stage may vary over 2 orders of magnitude, depending not only on the caldera d/s ratio, but also on d and s. Therefore, a simple relation between caldera maturity and erupted volumes is not the rule.

5.3. Regional tectonic control

The experiments have shown that the structure and development of a caldera is independent from pre-existing regional structures (Acocella et al., 2004) or stresses (Holohan et al., 2005). However, in both cases an elliptical caldera, elongated parallel to the maximum direction of extension, forms from an initially subcircular (in map view) reservoir. Its expected maximum eccentricity $E = L_{min}/L_{max}$ (where L_{min} is the length of the minor axis of the ellipse and L_{max} the length of the major axis) is ~0.8. The ellipticity of a caldera with a subcircular reservoir can be thus ascribed to regional tectonics.

A further mechanism, which may develop elliptical calderas from subcircular reservoirs, is post-collapse faulting. Regional normal faults may modify a subcircular caldera, elongating it according to the regional extension. This mechanism, even though not modelled, has been proposed for the elliptical Fieale caldera, Afar (De Chabalier and Avouac, 1994). However, its efficiency appears limited, as subvertical or highly dipping faults do not decrease caldera eccentricity of more than ~5% (Acocella et al., 2002).

Regional structures may modify subcircular calderas shaping the reservoir itself, producing an elliptical caldera above an elliptical reservoir. Various processes may produce elliptic reservoirs; a common one is similar to what observed at borehole breakouts, where the maximum regional compression reshapes the cavity, elongating it parallel to the least horizontal stress. This may explain the elongation, parallel to the regional extension, of calderas along the East African Rift System (Bosworth et al., 2000, 2003). A further process leading to elliptical calderas from elongated reservoirs is the deep intrusion of pre-existing regional structures. These may, especially when subvertical, constitute preferred pathways during the rise and emplacement of magma along the rift axis, enhancing its accumulation along a trend different from that of regional extension. The pre-existing discontinuities may act as feeder dikes of laccolith-like reservoirs beneath calderas

(Aizawa et al., 2006), as suggested for some calderas along the Ethiopian Rift (Acocella et al., 2002).

Therefore, in the first four proposed cases, regional tectonics is always responsible for calderas elongated parallel to the least compressive stress $\sigma 3$. These are common in, for example, the oceanic ridge of Iceland, East African Rift System, Taupo Volcanic Zone (New Zealand) and Western United States (Fig. 28). Conversely, only the latter mechanism, that is the control of pre-existing structures, may form calderas elongated with orientations different than the regional $\sigma 3$.

The frequency of elliptic calderas as a function of the angle α (between the caldera major axis and the regional structures trend) is shown in Fig. 29, in which 57 worldwide elliptic calderas, whose eccentricity $E < 0.9$, have been considered. Most (49%) calderas are perpendicular (or subperpendicular) to the regional (rift) structures controlling volcanism; 5% are oblique to the rift structures, but always parallel to significant pre-existing structures and 42% are parallel (or subparallel) to the rift structures.

The first four mechanisms proposed here (two of them experimentally tested) explain why elliptic calderas are mostly elongated parallel to the regional extension. The remaining mechanism (pre-existing structures controlling reservoir development) may explain the moderate number of calderas elongated obliquely to the regional structures. It may also explain the significant number of calderas elongated parallel to the main rift structures. These may control the elongation of the underlying reservoirs, constituting preferred pathways for the rise and emplacement of magma, similar to that proposed for pre-existing structures.

5.4. Possible limitations in the comparison to natural calderas

The underpressure experiments may be used to evaluate the structure and evolution of calderas. However, their application to any specific natural case should take into account possible limitations.

The major experimental limitation concerns the lack of a thermal gradient. It is not possible to define whether a specific thermal profile may affect the results. Variations in the dip of the ring faults may be, in principle, expected simulating a hot chamber and a ductile crust undergoing collapse. These may alter the proportions between the extent of the collapsed area and the chamber width. Another experimental limitation regards the possible role played by pre-existing structures related to regional tectonics. Regional pre-existing structures have been simulated only using subparallel 60° inward dipping faults (Acocella et al., 2004) and a throughout
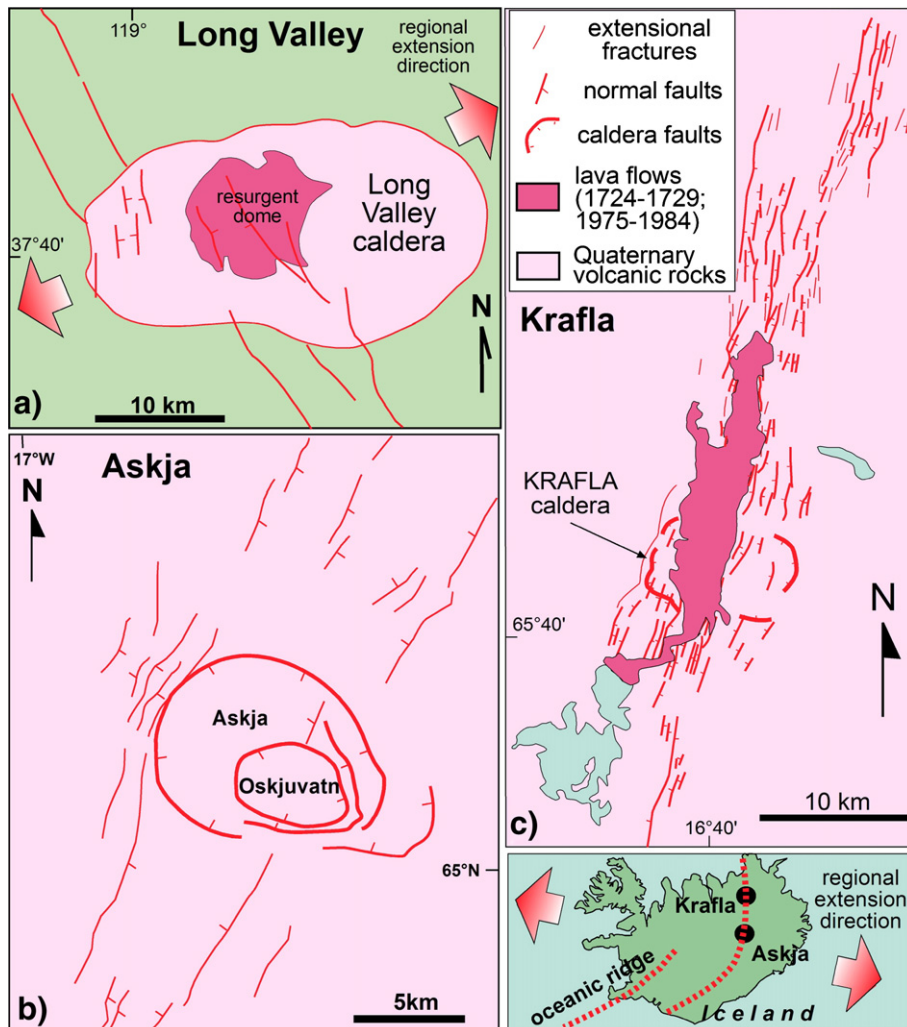
Fig. 28. Examples of elliptic calderas elongated accordingly with the regional extension. (a) Long Valley caldera, California, to the W of the Basin and Range extensional Province (after Goldstein and Stein, 1988). (b) Simplified structural map of Askja caldera, along the oceanic ridge of Iceland (modified after Sturkell and Sigmundsson, 2000). (c) Structural setting of Krafla (modified after Opheim and Gudmundsson, 1989). Inset at the bottom right shows the regional extension direction in Iceland.

investigation, taking into account also subvertical and outward dipping fractures, is needed.

A further limitation relates to the knowledge and correct definition of the surface structure of a caldera, from which the subsurface structure has to be inferred. This should lead to the definition of the caldera evolutionary stage. Wrong identifications of the surface structure of a caldera lead to wrong evaluations of its evolutionary stage. The surface structure of the natural calderas in Table 3 is based on previous studies, which describe their general shallow structure. In fact, the maturity of a caldera can be appreciated only considering its overall structure, even neglecting possible local complications or details.

Finally, multicyclic calderas characterized by repeated and partly overlapping collapses (as Las Canadas caldera,

Canarias; Martì and Gudmundsson, 2000; Martì et al., 1997, 2000) may introduce additional complications in the correct evaluation of their structure and should be analysed with particular care.

6. Implications for syn- and post-collapse volcanism and ore exploitation

During caldera formation, volcanism may be controlled by the amount of subsidence and the roof aspect ratio A. The overall relationships between caldera formation, volume of erupted magma and amount of subsidence have been highlighted in Section 5.2 (Fig. 27). As far as the roof aspect ratio is concerned, when $A < 1$, the volume variation within the reservoir during collapse is
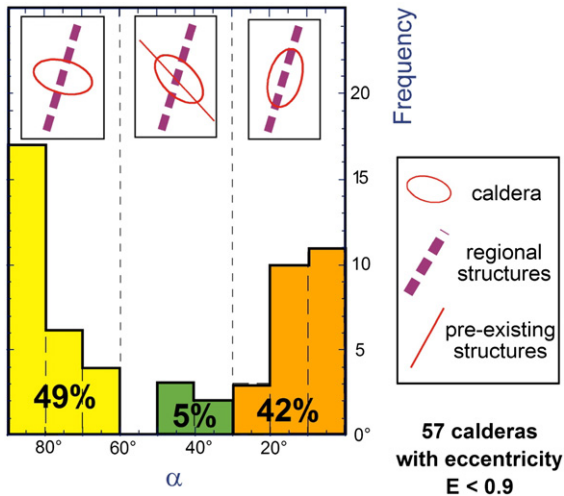
Fig. 29. Frequency distribution of 57 worldwide elliptic calderas, with eccentricity $E<0.9$, as a function of the angle α (between the caldera major axis and the trend of the regional structures).

similar to that of the depression created at the surface (Acocella et al., 2000; Roche et al., 2000). This implies is a $\sim 1:1$ ratio between the volumes of the caldera and the chamber contraction. Conversely, when $A>1$, the volume variation in the chamber is, in general, significantly lower than the volume of the caldera at surface, because of the incoherent deformation developed in the thicker roof (Roche et al., 2000). Therefore, the ratio between the caldera and chamber volumes becomes <1, implying that significant volumes of magma must be extruded to have collapse at surface. This is consistent with theoretical calculations (Roche and Druitt, 2001) and recent experiments (Geyer et al., 2006). Such a control of the roof aspect ratio may provide an explanation for the general occurrence of moderate effusive eruptions generating collapses at basaltic calderas and the higher volumes of explosive eruptions required to generate collapses at andesitic–dacitic–rhyolitic calderas (Cole et al., 2005, and references therein). In fact, several silicic calderas related to significant volume fractions of erupted magma, as Katmai, Ceboruco and Pinatubo, are associated with $A>1$ (Geyer et al., 2006 and references therein).

Post-collapse volcanism may similarly depend on the amount of subsidence and, subsequently, the roof aspect ratio. A moderate subsidence generates a downsag and no ring fault reaches the surface. Withdrawal of magma is expected along the vent responsible for the collapse and/or pre-existing structures or newly-formed fractures controlled by regional tectonics. Therefore, an understanding of the tectonic setting of a downsag caldera allows possible locations for vents to be predicted during unrests. With larger subsidence, the roof aspect ratio A becomes

important. If $A<1$, the ring faults reach the surface and the caldera structure itself may provide an effective (significant and/or fast) withdrawal of magma. In this case, the outward dipping ring fault, in stage 2 to 4 calderas, can be preferably intruded during post-collapse activity. In fact, the initial intrusion of magma along its deeper parts may depressurise the nearby portion of the chamber, inducing the sinking of its roof and triggering a feedback between magma intrusion along the fault and roof collapse (Fig. 30a to c). Conversely, the intrusion along the outer inward dipping ring fault, in stage 4 calderas, requires a higher energy, as a larger part of the caldera roof has to be uplifted, against gravity (Fig. 30d). This may explain the
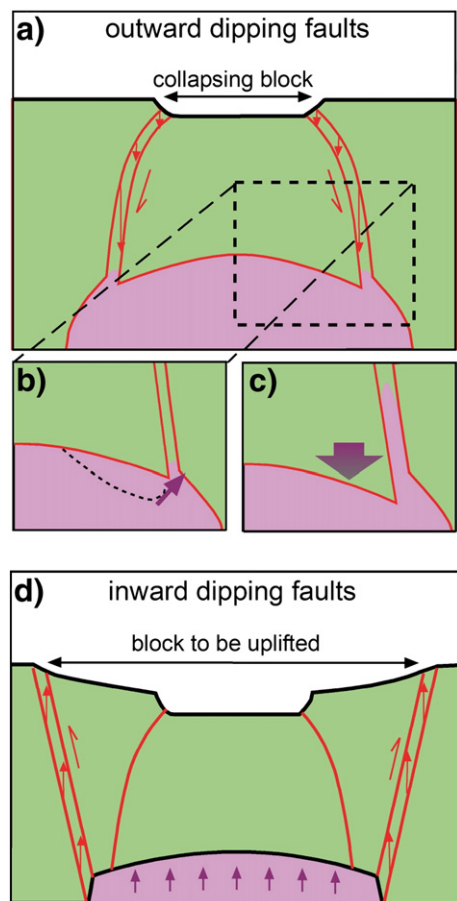

Fig. 30. (a) to (c) Possible role of the outward dipping reverse faults, in stage 2 to 4 calderas with roof aspect ratio $A<1$, in enhancing a feedback between magma intrusion and collapse: intrusion along the deeper ring fault depressurises the nearby reservoir (dashed area in b), inducing subsidence of the above roof and opening of the fault (c); magma may intrude further, progressively involving larger collapsing volumes. (d) The possibility to intrude inward dipping normal faults is less likely, as it involves the uplift, against gravity, of larger crustal portions.

common occurrence of post-caldera vents along the inner or outward dipping ring fault, at stage 2 (Deception Island; Walker, 1984), stage 3 (Rotorua; Milner et al., 2002) and stage 4 calderas (Valles, Campi Flegrei, Latera, Rabaul, Creede, Batur, Suswa; Lipman, 1984; Walker, 1984, and references therein; Newhall and Dzurisin, 1988; Nappi et al., 1991; Skilling, 1993; Di Vito et al., 1999). Possible variations to this behaviour are related to the opening of vents along additional regional or pre-existing structures, as at Bolsena, Hakone, Roccamonfina (Walker, 1984; Nappi et al., 1991; De Rita and Giordano, 1996). If $A > 1$, multiple sets of outward dipping reverse faults, defining an incoherent collapse, are expected (Roche et al., 2000) and the caldera structure may not provide such an effective withdrawal during post-collapse volcanism.

Calderas are also often associated with ore deposits, including porphyry Cu, epithermal, polymetallic veins and volcanogenic massive sulfide deposits (e.g. Burnham, 1979, 1985; Stix et al., 2003). In fact, the magma within the chamber provides a large source of heat and magmatic volatiles to drive hydrothermal systems. The resulting ore deposits may be located at different crustal levels between the magma chamber and the surface. The most suitable conditions for the rise of heated volatiles up to shallower crustal levels are met along preferred pathways, as pre-existing regional structures (e.g. Eddy et al., 1998; Smith et al., 2006) or, more commonly, caldera structures (e.g. Stix et al., 2003). There is widespread evidence that most mineralization at calderas clusters along the ring faults (Rytuba, 1994). At nested calderas, ore deposits along the outer ring system are common (Castor and Henry, 2000; Guillou Frottier et al., 2000, and references therein; Pals and Spry, 2003). However, there is particularly robust evidence for mineralization (especially volcanogenic massive sulfide deposits) in correspondence with the inner ring system, coinciding with the outward dipping reverse faults (Lexa et al., 1999; Guillou Frottier et al., 2000, and references therein; Mueller and Mortensen, 2002; Pals and Spry, 2003; Stix et al., 2003; Mueller et al., in press). This suggests that the location of the post-collapse mineralization may be explained, to a significant extent, by the caldera structure. In particular, the abundant ore deposits along the outward dipping reverse faults confirm that these may be easily permeated also by the volatiles of the hydrothermal system, even at shallow levels (Fig. 30).

Knowing the preferred pathways followed by the hydrothermal fluids is important also to properly understand the nature of ground deformation at calderas during unrests, as this may largely result from pressure variations within the hydrothermal system (e.g. Battaglia et al., 2006; De Vivo and Lima, 2006).

7. Towards a new caldera classification

The underpressure experiments and their comparison with calderas worldwide suggest an original revision of the structure, development and relationships of the established caldera types: downsag, piston-type, funnel, trapdoor and piecemeal (Lipman, 1997; Cole et al., 2005, and references therein). In fact, the consistency among experiments and nature suggests that the architecture and development of the caldera end-members described in the literature may be contextualised within a subsidence continuum (Fig. 31), in which the established caldera types are related to contributory factors (roof aspect ratio, symmetries, pre-existing faults; Acocella, 2006b).

Downsag calderas (experimental stage 1) are the first step in collapse, forming under limited subsidence. Most collapses will pass through the downsag phase, explaining the moderate number of natural downsag calderas. The increase in subsidence develops a stage 2 piston or funnel caldera, with roof aspect ratios $A < 1$ or $A > 1$ respectively (Roche et al. 2000). As funnels are usually accompanied by gravitational slumping (Lipman, 1997), they may be more frequent during advanced subsidence (Fig. 31). Increasing the subsidence further forms a peripheral downsag (stage 3), distinguished from that of stage 1 by the smaller d/s ratio (approximately $14 < d/s < 18$; Fig. 27). The latest stage (4) is characterized by two nested collapses.

Trapdoor calderas are asymmetric features and may form during stages 2 to 4. With higher d/s values, a
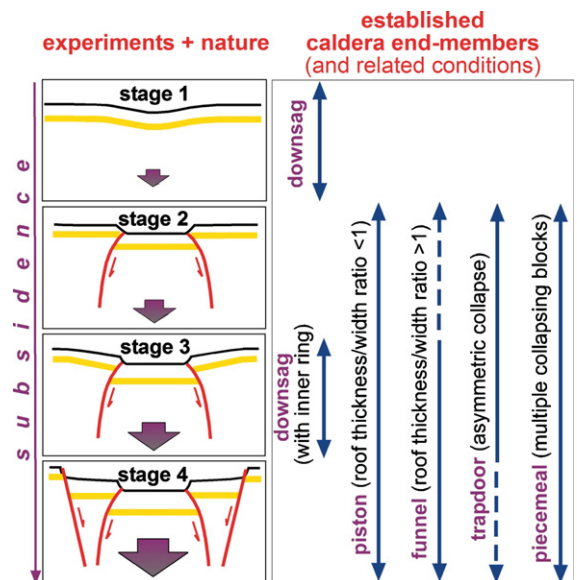

Fig. 31. Evolution of natural calderas geometries, summarized in 4 stages from a combination of experimental data and actual examples. To the right, caldera end-members (Lipman, 1997; Cole et al., 2005) and related conditions to form.

downsag forms on one side and a fault on the opposite (stage 2). Lower d/s values may form a reverse fault on the downsagged side and a normal fault on the opposite (stage 4). Fully developed stage 4 calderas should not be trapdoor, as the downsag should be replaced by the outer ring fault (Fig. 21).

Piecemeal is the only established caldera end-member that may have not been satisfactorily simulated experimentally; it has been obtained during inflation-deflation cycles (Troll et al., 2002), but not during the reactivation of regional structures (Acocella et al., 2004), as suggested by field data (Moore and Kokelaar, 1998). However, this discrepancy is apparent, as: a) piecemeal natural calderas are rare (Lipman, 1997); b) subsidence in the type piecemeal calderas (Glencoe, Scafell) is mainly achieved by downsag and, subsequently, slip along few faults (as "a" and "b" in Fig. 3c; Branney and Kokelaar, 1994; Moore and Kokelaar, 1998), whose location is similar to that of the experimental faults; c) in the type piecemeal calderas, only a minor subsidence is effectively accommodated along the multiple blocks (Fig. 3c; Branney and Kokelaar, 1994; Moore and Kokelaar, 1998). As natural piecemeals largely collapse through the same structures developed in the experiments, the models prove valid enough to understand also their overall architecture. Since piecemeal calderas require at least some significant faulting, they may belong to any of the last three evolutionary stages (Fig. 31).

More than one end-member may correspond to a certain evolutionary stage (Fig. 31). While a caldera stage is precisely defined by its structural features (Fig. 21), elements from caldera end-members (Fig. 31, right portion) are not diagnostic of the collapse stage. Therefore, the 5 established caldera end-members can be reconciled with the 4 evolutionary stages of calderas (Fig. 31), allowing an original classification which relies on the evolution and amount of subsidence of a caldera, identifying it accordingly with its overall surface structure. This classification not only incorporates the geometric, but more importantly, also the genetic features of calderas.

8. Conclusions

This overview of the analogue models of calderas identifies the following aspects on their structure and evolution:

1) The experiments simulating an overpressure within the reservoir, even if in agreement, require unrealistic uplifts to develop depressions; therefore, they do not explain most natural calderas.

2) All the experiments simulating calderas resulting from underpressure within the reservoir point to a consistent scenario defining the evolution and structure of calderas, regardless of any experimental boundary condition (materials, apparatus, scaling, volcanic edifices, regional stresses). These models may constitute a suitable analogue.

3) In underpressure experiments, caldera collapse develops in 4 stages, proportional to the amount of subsidence, progressively characterized by a: a) downsag, b) reverse ring fault; c) peripheral downsag, d) peripheral normal ring fault.

4) Most of the available geological and geophysical data at known calderas are consistent with the experimental structural features, as well as with their progression.

5) This consistency between experiments and geological–geophysical data has two main implications: (a) the experiments allow an understanding of the subsurface structure of natural calderas by knowing their surface structure; (b) considering the surface structure of calderas it may be possible to discriminate their deeper structure and belonging to any of the 4 experimental stages.

6) Several calderas, with a defined overall structure, may be suitable natural examples of these 4 stages, defining caldera types along a subsidence continuum. Many other natural calderas, when their surface structure is sufficiently known, may be reconciled with any of the 4 evolutionary stages, to infer their subsurface structure. The obtained relationship between the evolutionary stage of a caldera and its d/s (diameter/subsidence) ratio shows that stage 1 calderas are characterized by d/s > 40, stage 2 by 18 < d/s < 40, stage 3 by 14 < d/s < 18 and stage 4 by d/s < 14. The consistency between experiments and nature suggests that, in principle, the d/s ratio may permit to evaluate the overall structure and evolutionary stage of a caldera even when its surface structure is poorly known.

7) While the d/s ratio has an overall relation with the evolutionary stage of a caldera, it may be independent of the volume of erupted magma. However, the location of syn- and post-collapse volcanism may depend not only upon the amount of collapse, but also on the roof aspect ratio.

8) The experiments may explain the ellipticity of a part of natural calderas elongated parallel to the regional extension, while the control of pre-existing structures, though not simulated, may explain the elongation of elliptic calderas oblique or parallel to the regional structures.

9) The evolutionary stages explain the architecture and development of the established caldera end-members

along a continuum, where one or more end-members may correspond to a specific stage. While such a continuum is defined by precise structural features, controlled by progressive subsidence, specific geometries result from secondary factors (roof aspect ratio, collapse symmetry, pre-existing faults), not diagnostic of the collapse stage. These considerations allow proposing an original classification of calderas, incorporating their structural and genetic features.

Acknowledgements

References

Acocella, V., 2000. Space accommodation by roof lifting during pluton emplacement at Amiata (Italy). Terra Nova 12, 149–155.

Acocella, V., 2006a. Regional and local tectonics at Erta Ale caldera, Afar (Ethiopia). Journal of Structural Geology 28, 1808–1820.

Acocella, V., 2006b. Caldera types: How end-members relate to evolutionary stages of collapse. Geophysical Research Letters 33, L18314. doi:10.1029/2006GL027434.

Acocella, V., Faccenna, C., 2007. Structural features of the Campi Flegrei Caldera (Italy). Unpublished INGV-DPC (V3–2) report, Dipartimento Protezione Civile, Roma.

Acocella, V., Funiciello, R., 2006. Transverse systems along the extensional Tyrrhenian margin of central Italy and their influence on volcanism. Tectonics 25, TC2003. doi:10.1029/2005TC001845.

Acocella, V., Mulugeta, G., 2002. Experiments simulating surface deformation induced by pluton emplacement. Tectonophysics 352, 275–293.

Acocella, V., Cifelli, F., Funiciello, R., 2000. Analogue models of collapse calderas and resurgent domes. Journal of Volcanology and Geothermal Research 104, 81–96.

Acocella, V., Cifelli, F., Funiciello, R., 2001a. The control of overburden thickness on resurgent domes: insights from analogue models. Journal of Volcanology and Geothermal Research 111, 137–153.

Acocella, V., Cifelli, F., Funiciello, R., 2001b. Formation and architecture of nested collapse calderas: insights from analogue models. Terra Nova 13, 58–63.

Acocella, V., Korme, T., Salvini, F., Funiciello, R., 2002. Elliptic calderas in the Ethiopian Rift: control of pre-existing structures. Journal of Volcanology and Geothermal Research 119, 189–203.

Acocella, V., Funiciello, R., Marotta, E., Orsi, G., de Vita, S., 2004. The role of extensional structures on experimental calderas and resurgence. Journal of Volcanology and Geothermal Research 129, 199–217.

Aizawa, K., Acocella, V., Yoshida, T., 2006. How the development of magma chambers affects collapse calderas: insights from an overview. Journal of the Geological Society of London 269, 65–81.

Almond, D.C., 1977. Sabaloka igneous complex, Sudan. Philosophical Transactions of the Royal Society of London. Series A 287 (1348), 595–633.

Aramaki, S., 1984. Formation of the Aira caldera, Southern Kyushu, approximately 22.000 years ago. Journal of Geophysical Research 89, 8485–8501.

Aramaki, S., Takahashi, M., Nozawa, T., 1977. Kumano acidic rocks and Okueyama complex: two examples of granitic rocks in the outer zone of southwestern Japan. In: Yamada, N. (Ed.), Plutonism in relation to volcanism and metamorphism, proceedings of the 7th Circum-Pacific Plutonism Project Meeting. International Geological Correlation Program, UNESCO, Toyama, Japan, pp. 127–147.

Arana, V., Camacho, A.G., Garcia, A., Montesinos, F.G., Blanco, I., Vieira, R., Felpat, A., 2000. Internal structure of Tenerife (Canary Islands) based on gravity, aeromagnetic and Volcanological data. Journal of Volcanology and Geothermal Research 103, 43–64.

Bai, C., Greenlangh, S., 2005. 3D multi-step travel time tomography: imaging the local, deep velocity structure of Rabaul volcano, Papua New Guinea. Physics of the Earth and Planetary Interiors 151, 259–275.

Bailey, R.A., Dalrymple, G.B., Lanphere, M.A., 1976. Volcanism, structure, and geochronology of Long Valley Caldera, Mono County, California. Journal of Geophysical Research 81, 725–744.

Barberi, F., Cassano, E., La Torre, P., Sbrana, A., 1991. Structural evolution of Campi Flegrei caldera in light of Volcanological and geophysical data. Journal of Volcanology and Geothermal Research 48, 33–49.

Barberi, F., Buonasorte, G., Cioni, R., Fiordalisi, A., Foresi, L., Iaccarino, S., Laurenzi, M.A., Sbrana, A., Vernia, L., Villa, I.M., 1994. Plio-Pleistocene geological evolution of the geothermal area of Tuscany and Latium. Memorie Descrittive Della Carta Geologica d'Italia XLIX, 77–134.

Battaglia, M., Troise, C., Obrizzo, F., Pingue, F., De Natale, G., 2006. Evidence for fluid migration as the source of deformation at Campi Flegrei caldera (Italy). Geophysical Research Letters 33, L1307. doi:10.1029/2005GL024904.

Bellier, O., Sebrier, M., 1994. Relationship between tectonism and volcanism along the Great Sumatran fault Zone deduced by spot image analyses. Tectonophysics 233, 215–231.

Bellucci, F., Milia, A., Rolandi, G., Torrente, M.M., 2006. Structural control on the Upper Pleistocene ignimbrite eruptions in the Neapolitan area (Italy): volcano-tectonic faults versus caldera faults. In: De Vivo, B. (Ed.), volcanism in the Campania Plain: Vesuvius, Campi Flegrei and Ignimbrites. Developments in Volcanology, vol. 9, pp. 163–180.

Belousov, A., Walter, T.R., Troll, V.R., 2005. Large scale failures on domes and stratocones situated on caldera ring faults: sand-box modelling of natural examples from Kamchatka, Russia. Bulletin of Volcanology 67, 457–468.

Bosworth, W., Burke, K., Strecker, M., 2000. Magma chamber elongation as an indicator of intraplate stress field orientation: "borehole breakout mechanism" and examples from the Late Pleistocene to Recent Kenya Rift Valley. In: Jessel, M.W., Urai, J.L. (Eds.), Stress, Strain and Structure, a volume in honour of W.D. Means. Journal of the Virtual Explorer, vol. 2.

Bosworth, W., Burke, K., Strecker, M., 2003. Effect of stress fields on magma chamber stability and the formation of collapse calderas. Tectonics 22 (4), 1042. doi:10.1029/2002TC001369.

Branney, M.J., 1995. Downsag and extension at calderas: new prospectives on collapse geometries from ice-melt, mining, and volcanic subsidence. Bulletin of Volcanology 57, 303–318.

Branney, M.J., Gilbert, J.S., 1995. Ice-melt collapse pits and associated fractures in the 1991 lahar deposits of Volcan Hudson, Chile, criteria to distinguish eruption-induced glacier melt. Bulletin of Volcanology 57, 293–302.

Branney, M.J., Kokelaar, P., 1994. Volcanotectonic faulting, soft-state deformation and rheomorphism of tuffs during development of a piecemeal caldera, English lake District. GSA Bulletin 106, 507–530.

Burnham, C.W., 1979. Magma and hydrothermal fluids. In: Barnes, H.L. (Ed.), Geochemistry of hydrothermal ore deposits. Wiley, New York, pp. 71–136.

Burnham, C.W., 1985. Energy release in subvolcanic environments: implication for breccia formation. Economic Geology 80, 1515–1522.

Burov, E.B., Guillou-Frottier, L., 1999. Thermomechanical behaviour of large ash flow calderas. Journal of Geophysical Research 104, 23081–23109.

Cailleau, B., Walter, T.R., Janle, P., Hauber, E., 2003. Modeling volcanic deformation in a regional stress field: implications for the formation of graben structures on Alba Patera, Mars. Journal of Geophysical Research 108 (E12), 5141. doi:10.1029/2003JE002135.

Camacho, A.G., Vieira, R., de Toro, C., 1991. Microgravimetric model of the Las Canadas caldera (Tenerife). Journal of Volcanology and Geothermal Research 47, 75–88.

Capaccioni, B., Nappi, G., Renzulli, A., Santi, P., 1987. The eruptive history of Vepe Caldera (Latera volcano): a model inferred from structural and geochemical data. Periodico di Mineralogia 56, 269–283.

Carle, S.F., 1988. Three dimensional gravity modelling of the geologic structure of Long Valley caldera. Journal of Geophysical Research 93, 13237–13250.

Carter, A., van Wyk de Vries, B., Kelfoun, K., Bachelery, P., Briole, P., 2007. Pits, rifts and slumps: the summit structure of Piton de la Fournaise. Bulletin of Volcanology 69, 741–756.

Castor, S.B., Henry, C.D., 2000. Geology, geochemistry and origin of volcanic rock-hosted uranium deposits in northwestern Nevada and southeastern Oregon, USA. Ore Geology Reviews 16, 1–40.

Cespuglio, G., Campus, P., Sileny, J., 1996. Seismic moment tensor resolution by waveform inversion of a few local noisy records — II application to the Phlegraean Fields (Southern Italy) volcanic tremors. Geophysical Journal International 126, 620–634.

Chadwick, W.W., Howard, K.A., 1991. The pattern of circumferential and radial eruptive fissures on the volcanoes of Fernandina and Isabela islands, Galapagos. Bulletin of Volcanology 53, 259–275.

Cole, J.W., 1990. Structural control and origin of volcanism in the Taupo volcanic zone, New Zealand. Bulletin of Volcanology 52, 445–459.

Cole, J.W., Milner, D.M., Spinks, K.D., 2005. Calderas and caldera structures: a review. Earth Science Reviews 69, 1–96.

Davy, B., Bibby, H., 2005. Seismic reflection imaging of the Haraharo caldera boundary beneath Tarawera, Okataina volcanic centre, New Zealand. New Zealand Journal of Geology and Geophysics 48, 153–166.

Davy, B.W., Caldwell, T.G., 1998. Gravity, magnetic and seismic surveys of the caldera complex, Lake Taupo, North Island, New Zealand. Journal of Volcanology and Geothermal Research, 81, 69–89.

De Chabalier, J.B., Avouac, J.P., 1994. Kinematics of the Asal Rift (Djibouti) determined from the deformation of Fieale Volcano. Science 265, 1677–1681.

De Rita, D., Giordano, G., 1996. Volcanological and structural evolution of Roccamonfina volcano (Italy): origin of the summit caldera. In: McGuire, W.J., Jones, A.P., Neuberg, J. (Eds.), Volcano instability on the Earth and other planets. Geological Society Special Publications, vol. 110, pp. 209–224.

De Silva, S.L., 1989. Altiplano-Puna volcanic complex of the central Andes. Geology 17, 1102–1106.

De Vivo, B., Lima, A., 2006. A hydrothermal model for ground movements (bradyseism) at Campi Flegrei, Italy. In: De Vivo, B. (Ed.), Volcanism in the Campania Plain: Vesuvius, Campi Flegrei and Ignimbrites. Developments in Volcanology, vol. 9, pp. 289–317.

De Vivo, B., Rolandi, G., Gans, P.B., Calvert, A., Bohrson, W.A., Spera, F.J., Belkin, H.E., 2001. New constraints on the pyroclastic eruptive history of the Campanian volcanic Plain (Italy). Mineralogy and Petrology 73, 47–65.

Di Filippo, M., 1993. Sabatini Volcanic Complex. C.N.R., Roma, p. 109.

Di Vito, M.A., Isaia, R., Orsi, G., Southon, J., de Vita, S., D'Antonio, M., Pappalardo, L., Piochi, M., 1999. Volcanism and deformation since 12000 years at the Campi Flegrei caldera (Italy). Journal of Volcanology and Geothermal Research 91, 221–246.

Donnadieu, F., Merle, O., 1998. Experiments on the indentation process during cryptodome intrusions: new insights into Mount St. Helens deformation. Geology 26, 79–82.

Druitt, T.H., Sparks, R.S., 1984. On the formation of calderas during ignimbrite eruptions. Nature 310, 679–681.

Eddy, C.A., Dilek, Y., Hurst, S., Moores, E.M., 1998. Seamount formation and associated caldera complex and hydrothermal mineralization in ancient oceanic crust, *Troodos ophiolite* (Cyprus). Tectonophysics 292, 189–210.

Florio, G., Fedi, M., Cella, F., Rapolla, A., 1999. The Campanian Plain and Phlegrean Fields: structural setting from potential field data. Journal of Volcanology and Geothermal Research 91, 361–379.

Folch, A., Martì, J., 2004. Geometrical and mechanical constraints on the formation of ring fault calderas. Earth and Planetary Science Letters 221, 215–225.

Fridrich, C.J., Mahood, G.A., 1984. Reverse zoning in the resurgent intrusions of the Grizzly Peak cauldron, Sawatch Range, Colorado. Geological Society of America Bulletin 95, 779–787.

Fridrich, C.J., Smith, R.P., De Witte, E., McKee, E.H., 1991. Structural, eruptive, and intrusive history of the Grizzly Peak caldera, Sawatch range, Colorado. GSA Bulletin 103, 1160–1177.

Geshi, N., Shimano, T., Chiba, T., Nakada, S., 2002. Caldera collapse during the 2000 eruption of Miyakejima volcano, Japan. Bulletin of Volcanology 64, 55–68.

Geyer, A., Folch, A., Martì, J., 2006. Relationship between caldera collapse and magma chamber withdrawal: an experimental approach. Journal of Volcanology and Geothermal Research 157, 375–386.

Giordano, G., De Benedetti, A.A., Diana, A., Diano, G., Gaudioso, F., Marasco, F., Miceli, S., Mollo, S., Cas, R.A.F., Funiciello, R., 2006. The Colli Albani mafic caldera (Roma, Italy): stratigraphy, structure and petrology. Journal of Volcanology and Geothermal Research 155, 49–80.

Goldstein, N.E., Stein, R.S., 1988. What's new at Long Valley. Journal of Geophysical Research 93, 13,187–13,190.

Gray, J.P., Monaghan, J.J., 2004. Numerical modelling of stress fields and fracture around magma chambers. Journal of Volcanology and Geothermal Research 135, 259–283.

Gudmundsson, A., 1988. Formation of collapse calderas. Geology 16, 808–810.

Gudmundsson, A., 1998a. Magma chambers modeled as cavities explain the formation of rift zone central volcanoes and their eruption and intrusion statistics. Journal of Geophysical Research 103, 7401–7412.

Gudmundsson, A., 1998b. Formation and development of normal fault calderas and the initiation of large explosive eruptions. Bulletin of Volcanology 60, 160–170.

Gudmundsson, A., 1999. Postglacial crustal doming, stresses and fracture formation with application to Norway. Tectonophysics 307, 407–419.

Gudmundsson, A., Nilsen, K., 2006. Ring faults in composite volcanoes: structures, models, and stress fields associated with their formation. Journal of the Geological Society of London 269, 83–108.

Gudmundsson, A., Marti, J., Turon, E., 1997. Stress fields generating ring faults in volcanoes. Geophysical Research Letters 24, 1559–1562.

Guidarelli, M., Zille, A., Saraò, A., Natale, M., Nunziata, C., Panza, G.F., 2006. Shear-wave velocity models and seismic sources in Campanian volcanic areas: Vesuvio and Campi Flegrei. In: Dobran, F. (Ed.), VESUVIUS 2000: Education, Security and Prosperity. Elsevier, Amsterdam, pp. 287–309.

Guillou Frottier, L., Burov, E.B., Milesi, J.-P., 2000. Genetic links between ash flow calderas and associated ore deposits as revealed by large-scale thermo-mechanical modeling. Journal of Volcanology and Geothermal Research 102, 339–361.

Hallinan, S., 1993. Nonchaotic collapse at funnel calderas: gravity study of the ring fractures at Guayabo caldera, Costa Rica. Geology 21, 367–370.

Hallinan, S., Brown, G., 1995. Incremental collapse and stratocone growth within a funnel-shaped caldera, Guayabo, Costa Rica. Journal of Volcanology and Geothermal Research 67, 101–122.

Henry, C.H., Price, J.G., 1984. Variations in caldera development in the Tertiary volcanic field of Trans-Pecos Texas. Journal of Geophysical Research 89, 8765–8786.

Holohan, E.P., Troll, V.R., Walter, T.R., Munn, S., McDonnell, S., Shipton, Z.K., 2005. Elliptical calderas in active tectonic settings: an experimental approach. Journal of Volcanology and Geothermal Research, 144, 119–135.

Hubbert, M.K., 1937. Theory of scale models as applied to the study of geologic structures. Bulletin of the Geological Society of America 48, 1459–1520.

Jonsson, S., Zebker, H., Amelung, F., 2005. On trapdoor faulting at Sierra Negra volcano, Galapagos. Journal of Volcanology and Geothermal Research 144, 59–72.

Kennedy, B., Styx, J., 2003. Igneous rock associations of Canada 2. Stages in the temporal evolution of calderas. Geoscience Canada 30, 129–140.

Kennedy, B., Styx, J., Vallance, J.W., Lavallèe, Y., Longprè, M.A., 2004. Controls on caldera structure: results from analogue sandbox modelling. GSA Bulletin 106, 515–524.

Komuro, H., 1987. Experiments on cauldron formation: a polygonal cauldron and ring fractures. Journal of Volcanology and Geothermal Research 31, 139–149.

Komuro, H., Fujita, Y., Kodama, K., 1984. Numerical and experimental models on the formation mechanism of collapse basins during the Green Tuff Orogenesis of Japan. Bulletin of Volcanology 47, 649–666.

Kuno, H., Oki, Y., Ogino, K., Hirota, S., 1970. Structure of Hakone caldera as revealed by drilling. Bulletin of Volcanology 34, 713–725.

Kusumoto, S., Takemura, K., 2003. Numerical simulation of caldera formation due to collapse of a magma chamber. Geophysical Research Letters 30, 2278. doi:10.1029/2003GL018380.

Kusumoto, S., Fukuda, Y., Takemura, K., 1999. A distinction technique between volcanic and tectonic depression structures based on the restoration modeling of gravity anomaly: a case study of the Hohi volcanic zone, central Kyushu, Japan. Journal of Volcanology and Geothermal Research 90, 183–189.

Lavallèe, Y., Stix, J., Kennedy, B., Richer, M., Longprè, M.A., 2004. The role of laboratory experiments in volcanology. Journal of Volcanology and Geothermal Research 129, 219–236.

Lexa, J., Stohl, J., Konecny, V., 1999. The Banska Stiavnica ore district: relationship between metallogenic processes and the geological evolution of a stratovolcano. Mineralium Deposita 34, 639–654.

Lindsay, J.M., De Silva, S., Trumbull, R., Emmermann, R., Wemmer, K., 2001. La Pacana caldera, N Chile: a re-evaluation of the stratigraphy and Volcanology of one of the world's largest resurgent calderas. Journal of Volcanology and Geothermal Research 106, 145–173.

Lipman, P.W., 1984. The roots of ash flow calderas in Western North America: windows into the tops of granitic batholiths. Journal of Geophysical Research 89, 8801–8841.

Lipman, P.W., 1997. Subsidence of ash-flow calderas: relation to caldera size and magma-chamber geometry. Bulletin of Volcanology 59, 198–218.

Lipman, P.W., 2003. Geometrically complex calderas and underlying magma chambers in the Western USA. Proceedings of the IUGG XXIII Assembly, Sapporo, Japan, pp. 526–527.

Mandl, G., 1988. Mechanics of tectonic faulting: models and basic concepts. Elsevier, Amsterdam. 401 pp.

Martì, J., Gudmundsson, A., 2000. The Las Canadas caldera (Tenerife, Canary Islands): Example of an overlapping collapse caldera generated by magma-chamber migration. Journal of Volcanology and Geothermal Research 103, 161–173.

Martì, J., Ablay, G.J., Redshaw, L.T., Sparks, R.S.J., 1994. Experimental studies of collapse calderas. Journal of the Geological Society (London) 151, 919–929.

Martì, J., Hurlimann, M., Ablay, G.J., Gudmundsson, A., 1997. Vertical and lateral collapses on Tenerife (Canary Islands) and other volcanic ocean islands. Geology 25, 879–882.

Martì, J., Folch, A., Neri, A., Macedonio, G., 2000. Pressure evolution during explosive caldera-forming eruptions. Earth and Planetary Science Letters 175, 275–287.

Merle, O., Vendeville, B., 1995. Experimental modelling of thin-skinned shortening around magmatic intrusions. Bulletin of Volcanology 57, 33–43.

Milner, D.M., Cole, J.W., Wood, C.P., 2002. Asymmetric, multiple block collapse at Rotorua caldera, taupo Volcanic Zone, New Zealand. Bulletin of Volcanology 64, 134–149.

Miura, D., 1999. Arcuate pyroclastic conduits, ring faults and coherent floor at Kumano caldera, southwest Honshu, Japan. Journal of Volcanology and Geothermal Research 92, 271–294.

Miura, D., 2005. Effects of changing stress states on the development of caldera-bounding faults: geological evidence from Kumano caldera, Japan. Journal of Volcanology and Geothermal Research 144, 89–103.

Miura, D., Tamai, M., 1998. Intracaldera structure and megabreccias at Dorobu caldera, northeastern Honshu, Japan. Journal of Volcanology and Geothermal Research 80, 195–215.

Mohr, P.A., Wood, C.A., 1976. Volcano spacing and lithospheric attenuation in the Eastern Rift of Africa. Earth and Planetary Science Letters 33, 126–144.

Montesinos, F.G., Camacho, A.G., Vieira, R., 1999. Analysis of gravimetric anomalies in Furnas caldera. Journal of Volcanology and Geothermal Research 92, 67–81.

Moore, I., Kokelaar, P., 1998. Tectonically controlled piecemeal caldera collapse: a case study of Glencoe volcano, Scotland. GSA Bulletin 110, 1448–1466.

Mori, J., Mckee, C., 1987. Outward-dipping ring-fault structure at Rabaul Caldera as shown by earthquake locations. Science 235, 193–195.

Mori, J., White, R., Harlow, D., Okubo, P., Power, J., Hoblitt, R., Laguerta, E., Lanuza, L., Bautista, B., 1996. Volcanic earthquakes following the 1991 climactic eruption of Mount Pinatubo, Philippines: strong seismicity during a waning eruption. In: Newhall C., Punongbayan R., Eds. Fire and Mud: Eruptions and Lahars of Mount Pinatubo, Philippines. PHIVOLCS and Univ. Washington Press, 339–350.

Mouginis-Mark, P.J., Rowland, S.K., 2001. The geomorphology of planetary calderas. Geomorphology 37, 201–223.

Mueller, W.U., Mortensen, J.K., 2002. Age constraints and characteristics of subaqueous volcanic construction, the Archean Hunter Mine Group, Abitibi greenstone belt. Precambrian Research 115, 119–152.

Mueller, W.U., Stix, J., White, J.D.L., Corcoran, P.L., Lafrance, B., Daigneault, R., in press. Characterisation of Archean subaqueous calderas in Canada: physical volcanology, carbonate-rich hydrothermal alteration and a new exploration model. In Caldera volcanism: analysis, modelling and response (Marti J., Gottsmann J., eds.). Developments in Volcanology, Elsevier.

Munro, D.C., Rowland, S.K., 1996. Caldera morphology in the western Galapagos and implications for volcano eruptive behaviour and mechanism of caldera formation. Journal of Volcanology and Geothermal Research 72, 85–100.

Nakajima, J., Hasegawa, A., 2003. Tomographic imaging of seismic velocity structure in and around the Onikobe volcanic area, northeastern Japan: implications for fluid distribution. Journal of Volcanology and Geothermal Research 127, 1–18.

Nappi, G., Renzulli, A., Santi, P., 1991. Evidence of incremental growth in the Vulsinian calderas (central Italy). Journal of Volcanology and Geothermal Research 47, 13–31.

Natale, M., Nunziata, C., Panza, G.F., 2005. Average shear wave velocity models of the crustal structure at Mt. Vesuvius. Physics of the Earth and Planetary Interiors 152, 7–21.

Newhall, C.G., Dzurisin, D., 1988. Historical unrest at large calderas of the world. U.S. Geological Survey. 1109 pp.

Nunziata, C., Natale, M., Luongo, G., Panza, G.F., 2006. Magma reservoir at Mt. Vesuvius: size of the hot, partially molten crust material detected deeper than 8 km. Earth and Planetary Science Letters 242, 51–57.

Odonne, F., Ménard, I., Massonnat, G.J., Rolando, J.P., 1999. Abnormal reverse faulting above a depleting reservoir. Geology 27, 111–114.

Okubo, C.H., Martel, S.J., 1998. Pit crater formation on Kilauea volcano, Hawaii. Journal of Volcanology and Geothermal Research 86, 1–18.

Opheim, J.A., Gudmundsson, A., 1989. Formation and geometry of fractures and related volcanism of the Krafla fissure swarm, Northeast Iceland. Geological Society of America Bulletin 101, 1608–1622.

Orsi, G., De Vita, S., di Vito, M., 1996. The restless, resurgent Campi Flegrei nested caldera (Italy): constrains on its evolution and configuration. Journal of Volcanology and Geothermal Research 74, 179–214.

Pals, D.W., Spry, P.G., 2003. Telluride mineralogy of the low-sulfidation epithermal Emperor gold deposit, Vatukoula, Fiji. Mineralogy and Petrology 79, 285–307.

Pinel, V., Jaupart, C., 2005. Caldera formation by magma withdrawal from a reservoir beneath a volcanic edifice. Earth and Planetary Science Letters 230, 273–287.

Ramberg, H., 1981. Gravity, deformation and the Earth's crust, 2nd ed. Academic Press, London. 452 pp.

Roche, O., Druitt, T.H., 2001. Onset of caldera collapse during ignimbrite eruptions. Earth and Planetary Science Letters 191, 191–202.

Roche, O., Druitt, T.H., Merle, O., 2000. Experimental study of caldera formation. Journal of Geophysical Research 105, 395–416.

Roche, O., van Wyk de Vries, B., Druitt, T.H., 2001. Sub-surface structures and collapse mechanisms of summit pit craters. Journal of Volcanology and Geothermal Research 105, 1–18.

Rolandi, G., Bellucci, F., Heizler, M., Belkin, H.E., De Vivo, B., 2003. Tectonic controls on the genesis of ignimbrites from the Campanian Volcanic Zone, Southern Italy. In: De Vivo, B., Scandone, R. (Eds.), Ignimbrites of the Campanian Plain, Italy. Mineralogy and Petrology, vol. 79, pp. 3–31.

Rosi, M., Sbrana, A., 1987. Phlegraean Fields. Quaderni Ricerca Scientifica, vol. 114. CNR, Roma. 167 pp.

Rowland, S.K., Munro, D.C., 1992. The caldera of Volcan Fernandina: a remote sensing study of its structure and recent activity. Bulletin of Volcanology 55, 97–109.

Rymer, H., van Wyk de Vries, B., Stix, J., William-Jones, G., 1998. Pit crater structure and processes governing activity at Masaya volcano, Nicaragua. Bulletin of Volcanology 59, 345–355.

Rytuba, J.J., 1994. Evolution of volcanic and tectonic features in caldera settings and their importance in the localization of ore-deposits. Economic Geology and the Bulletin of the Society of Economic Geologists 89, 1687–1696.

Rytuba, J.J., McKee, E.H., 1984. Peralkaline ash flow tuffs and calderas of the McDermitt Volcanic Field, Southeast Oregon and North Central Nevada. Journal of Geophysical Research 89, 8616–8628.

Sanford, A.R., 1959. Analytical and experimental study of simple geological structures. Bulletin of the Geological Society of America 70, 19–52.

Saunders, S.J., 2001. The shallow plumbing system of Rabaul caldera: a partially intruded ring fault? Bulletin of Volcanology 63, 406–420.

Scandone, R., Malone, S., 1985. Magma supply, magma discharge and readjustment of the feeding system of Mount St Helens during 1980. Journal of Volcanology and Geothermal Research 23, 239–262.

Schmincke, H.U., 1967. Cone sheet swarm, resurgence of Tejeda Caldera and the early geologic history of Gran Canaria. Bulletin of Volcanology 31, 153–162.

Self, S., Wolff, J., 2005. Outstanding issues about the relationships between large-scale calderas, ignimbrite volumes and magma body shape and longevity. Proceedings of the "Caldera volcansim: analysis, modelling and response" Workshop, Tenerife, Spain, pp. 15–16.

Self, S., Goff, F., Gardner, J.N., Wright, J.V., Kite, W.M., 1986. Explosive rhyolitic volcanism in the Jemez Mountains: vent locations, caldera development and relation to regional structure. Journal of Geophysical Research 91, 1779–1798.

Setterfield, T.N., Eaton, P.C., Rose, W.J., Sparks, S.J., 1991. The Tavua caldera, Fiji: a complex shoshonitic caldera formed by concurrent faulting and downsagging. Journal of the Geological Society of London 148, 115–127.

Skilling, I.P., 1993. Incremental caldera collapse of Suswa volcano, Gregory Rift Valley, Kenya. Journal of the Geological Society (London) 150, 885–896.

Simei, S., Acocella, V., Palladino, D., Trigila, R., 2006. Evolution and structure of Vulsini calderas (Italy). Proceedings of the 2006 EGU Assembly, Austria, Vienna.

Simkin, T., Howard, K.A., 1970. Caldera collapse in the Galapagos islands, 1968. Science 169, 429–437.

Smith, R.L., Bailey, R.A., 1968. Resurgent cauldrons. Geological Society of American Memoirs 116, 613–662.

Smith, R.B., Braile, L.W., 1994. The Yellowstone hotspot. Journal of Volcanology and Geothermal Research 61, 121–187.

Smith, N., Cassidy, J., Locke, C.A., Mauk, J.L., Christie, A.B., 2006. The role of regional-scale faults in controlling a trapdoor caldera, Coromandel Peninsula; New Zealand. Journal of Volcanology and Geothermal Research 149, 312–328.

Sollevanti, F., 1983. Geologic, volcanologic and tectonic setting of the Vico-Cimino area, Italy. Journal of Volcanology and Geothermal Research 17, 203–217.

Spinks, K., Acocella, V., Cole, J., Bassett, K., 2005. Structural control of volcanism and caldera development in the transtensional Taupo Volcanic Zone, New Zealand. Journal of Volcanology and Geothermal Research 144, 7–22.

Stix, J., Kennedy, B., Hannington, M., Gibson, H., Fiske, R., Mueller, W., Franklin, J., 2003. Caldera-forming processes and the origin of submarine volcanogenic massive sulfide deposits. Geology 31, 375–378.

Sturkell, E., Sigmundsson, F., 2000. Continuous deflation of the Askja caldera, Iceland, during the 1983–1998 noneruptive period. Journal of Geophysical Research 105, 25671–25684.

Sudo, Y., Kong, L.S.L., 2001. Three dimensional seismic velocity structure beneath Aso Volcano, Kyushu, Japan. Bulletin of Volcanology 63, 326–344.

Suemnicht, G.A., Varga, R.J., 1988. Basement structure and implications for hydrothermal cirulation patterns in the Western Moat of Long Valley caldera, California. Journal of Geophysical Research 93, 13191–13207.

Swanson, E.R., McDowell, F.W., 1984. Calderas of the Sierra Madre Occidental Volcanic Field, Western Mexico. Journal of Geophysical Research 89, 8787–8799.

Talbot, C.J., 1999. Can field data constrain rock viscosities? Journal of Structural Geology 21, 949–957.

Troll, V.R., Emeleus, C.H., Donaldson, C.H., 2000. Caldera formation in the Rum central Igneous Complex, Scotland. Bulletin of Volcanology 62, 301–317.

Troll, V.R., Walter, T.R., Schmincke, H.U., 2002. Cyclic caldera collapse: piston or piecemeal subsidence? Field and experimental evidence. Geology 30, 135–138.

Tucker, D., Hildreth, W., Ullrich, T., Friedman, R., 2007. Geology and complex collapse mechanisms of the 3.72 Ma Hannegan caldera, North Cascades, Washington, USA. Geological Society of America Bulletin 119, 329–342.

Turcotte, D.L., Schubert, G., 1982. Geodynamics: application of continuum physics to geological problems. John Wiley, NY. 450 pp.

Vezzoli, L., 1988. Island of Ischia. C.N.R., Rome. 135 pp.

Walker, G.P.L., 1984. Downsag calderas, ring faults, caldera sizes, and incremental caldera growth. Journal of Geophysical Research 89, 8407–8416.

Walter, T.R., Troll, V.R., 2001. Formation of caldera periphery faults: an experimental study. Bulletin of Volcanology 63, 191–203.

Williams, H., 1941. Calderas and their origin. Bulletin of the Department of Geological Sciences, University of California 21, 239–346.

Williams, L.A.J., MacDonald, R., Chapman, G.R., 1984. Late Quaternary caldera volcanoes of the Kenya Rift Valley. Journal of Geophysical Research 89, 8553–8570.

Worthington, T.J., Gregory, M.R., Bondarenko, V., 1999. The Denham caldera on Raoul volcano: dacitic volcanism in the Tonga-Kermadec arc. Journal of Volcanology and Geothermal Research 90, 29–48.

Wunderman, R.L., Rose, W.I., 1984. Amatitlan, an actively resurging cauldron 10 km south of Guatemala City. Journal of Geophysical Research 89, 8525–8539.

Yoshida, T., 1984. Tertiary Ishizuchi Cauldron, Southwestern Japan Arc: formation by Ring Fracture Subsidence. Journal of Geophysical Research 89, 8502–8510.

Yoshida, T., 2001. The evolution of arc magmatism in the NE Honshu arc, Japan. Tohoku Geophysical Journal 36, 131–249.

Zollo, A., Gasparini, P., Virieux, J., Le Meur, H., De Natale, G., Biella, G., Boschi, E., Capitano, P., de Franco, R., dell'Aversana, P., De Matteis, R., Guerra, I., Iannaccone, G., Mirabile, L., Vilardo, G., 1996. Seismic evidence for a low-velocity zone in the upper crust beneath Mount Vesuvius. Science 274, 592–594.

Zollo, A., Judenherc, S., Auger, E., D'Auria, L., Virieux, J., Captano, P., Chiarabba, C., De Franco, R., Ma kris, J., Nichelini, A., Musacchio, G., 2003. Evidence for the buried rim of Campi Flegrei caldera from 3-d active seismic imaging. Geophysical Research Letters 30. doi:10.1029/2003GL018173.